Chemical Technology and Engineering Applications

https://ctea.cultechpub.com/ctea

Cultech Publishing

Article

Synthesis, Characterization and Antimicrobial Studies of Benzophenone Oxime Derived from Benzophenone and Hydroxylamine and Its Metal(II) Complexes

Umar Jari[1], Junaidu Na'aliya[1], Ansar Bilyaminu Adam[2,*], Raymond Bwano Donatus[2], Ataitiya Hyelalibiya[2]

[1]Department of Pure and Industrial Chemistry, Bayero University Kano, Kano, Nigeria

[2]Department of Industrial Chemistry, Federal University Wukari, Wukari, Nigeria

[*]Corresponding author: Ansar Bilyaminu Adam, ansarbilyamin@gmail.com

Abstract

The synthesis of benzophenone oxime was done through the reaction of benzophenone with hydroxylamine hydrochloride and complexed with Mn(II), Fe(II), Co(II), Cu(II), Zn(II), and Cd(II) chlorides to produce the corresponding Metal(II) complexes. This ligand was produced in 87.43%, and its melting point is 128 °C, and the complexes were obtained in 60-75% yield with decomposition temperatures of 162-178 °C, which showed great thermal stability. The elemental analyses indicated a ligand-to-metal ratio of 2:1, and the values of molar conductance (13.27-29.63 $cm^2\ mol^{-1}$) indicated non-electrolytic behavior. The analysis of FTIR spectra revealed a C=N stretch at 1655 cm^{-1} in the ligand, which changed to 1595-1654 cm^{-1} in the complexes, with the new bands appearing at 430-506 cm^{-1}, indicating N,O-coordination. Mn(II), Fe(II), Co(II), and Cu(II) complexes were found to be paramagnetic with Mn(II), Fe(II), Co(II), and Cu(II), whereas Zn(II) and Cd(II) were found to be diamagnetic. The ligand exhibited $\pi \rightarrow \pi^*$ transitions at 250-320 nm and $n \rightarrow \pi^*$ transitions at 350-370 nm in the UV-vis spectra, and bathochromic shifts occurred in all the complexes. Mn(II) demonstrated the d-to-d bands at 400-600 nm, whereas Co and Cu resembled the ligand with broader bands at 500-600 nm, which can be attributed to d-to-d and ligand-to-metal charge transfer, respectively. Zn and Cd resembled the ligand, which is expected in the d^{10} kind of configurations. TGA showed an increase in thermal stability of all complexes with increased residual masses at 800 °C, indicating the formation of stable metal oxides. Antimicrobial activity of Cu(II) and Cd(II) complexes against *Staphylococcus aureus (S. aureus), Salmonella typhi (S. typhi) , Escherichia coli (E. coli), Candida albicans (C. albicans), and Aspergillus flavus (A. flavus)* indicated that complexes were more active than the free ligand. These results indicate the thermal stability of the complexes and possible pharmaceutical use, which awaits toxicity testing.

Keywords

Oxime ligand, Transition metal complexes, Coordination chemistry, Antimicrobial activity, Bioinorganic chemistry

Article History

Received: 27 November 2025
Revised: 05 January 2026
Accepted: 12 March 2026
Available Online: 30 March 2026

1. Introduction

Coordination describes the process or condition in which an atom, molecule, or ion is bound together. A significant issue in this context is the utilization of Schiff bases, often derived from the condensation of amines and carbonyl compounds. These compounds exhibit structural flexibility and robust binding with metal ions. Consequently, these compounds can function as effective ligands to form complexes with advantageous chemical and biological characteristics [1,2].

Schiff base metal complexes can either diminish or enhance the reactivity of the transition metal core. Additionally, they possess biological and chemical significance. These ligands enable the manipulation of the sphere surrounding the metal, facilitating alterations in its shape, oxidation state, and other properties. Regulation is crucial due to their utility in enzymatic mimics across various domains, magnetic materials, and biological applications, as noted by [3-5]. Integrating them into a chelation with transition metals results in a stable structure capable of enduring various physiological and environmental conditions.

Increasing interest is being generated in these Schiff base metal complexes due to global bacterial resistance to pharmaceuticals. Antibiotics are progressively losing their efficacy over time. Consequently, the examination of macrocyclic and heteroaromatic Schiff base ligands is underway for the advancement of medicinal medicines. Kajal et al. [6] and Sankar and Sharmila [7,8] assert that cannabis and other chemicals exhibit efficacy against bacteria, fungi, and cancers, necessitating their incorporation in the development of next, generation pharmaceuticals.

Schiff-base metal complexes are structurally robust and show a broad spectrum of biological activities, making them promising candidates for antimicrobial agents. In particular, octahedral complexes (and related coordination geometries) of zinc and cobalt have demonstrated inhibitory activity against common pathogens such as Staphylococcus aureus, Escherichia coli, and Klebsiella pneumoniae. Chelation often increases the lipophilicity of these complexes, which can enhance their ability to penetrate microbial cell membranes and reach intracellular targets. Consequently, coordination chemistry continues to explore Schiff-base-containing metal complexes to optimize structural features that improve antimicrobial potency and selectivity [9,10].

The current research proposes benzophenone oxime as a ligand to Mn(II), Fe(II), Co(II), Cu(II), Zn(II), and Cd(II) complexes, which provides certain originality over a conventional Schiff base or oxime metal system. In contrast to simpler ligands, benzophenone oxime offers a bulky aromatic structure that has an effect on coordination geometry, thermal stability, and biologic activity. FTIR, magnetic susceptibility, elemental analysis, and conductometric measurements all confirmed a 2:1 ligand-to-metal ratio with dual-site coordination via nitrogen and oxygen, as demonstrated by shifted C=N stretches and additional M-O vibrations. The complexes are thermally stable (decomposition temperatures of 162 and 178 °C) and have increased antimicrobial activity against a variety of bacterial and fungal strains, with the greatest effects observed with Cu(II) and Cd(II) complexes, which are more effective than the free ligand. The results not only point to basic understandings of both overall ligand and metal interactions and viable provision of potential applications in the pharmaceutical field, but they also make the present benzophenone-based system stand out compared to the previously described oxime-metal complexes.

The primary aim of this work was to examine the impact of transition metal chelation by Schiff base ligands on the coordination geometry, stability, and reactivity assessment of specific ligands against specified pathogenic bacteria, by linking structure to action or activity.

2. Materials and Methods

2.1 Materials

All reagents and solvents were employed in analytically pure condition and without the intervention of drying or distillation. Benzophenone and hydroxylamine hydrochloride were obtained from the Sigma, Aldrich catalogue.

2.2 Methods

2.2.1 Synthesis of the Ligand

Benzophenone oxime was synthesized following the method reported by Adaji et al. [1], based on the alkaline oximation of ketones. Benzophenone (1.82 g, 10 mmol) and hydroxylamine hydrochloride (1.04 g, 15 mmol) were dissolved in 20 cm^3 of absolute ethanol in a round-bottom flask. The suspension was heated at 50-60 °C for 5-10 minutes with continuous stirring. Sodium hydroxide (0.80 g, 20 mmol) was then added gradually to liberate free hydroxylamine and establish alkaline conditions. A fractional distillation condenser was attached, and the reaction mixture was refluxed for 3 h. After reflux, the solution was allowed to cool to room temperature and left undisturbed for 24 h to facilitate crystallization. The resulting shining crystalline product was collected by vacuum filtration, washed with cold absolute ethanol, and dried over anhydrous calcium chloride in a sealed desiccator prior to further characterization.

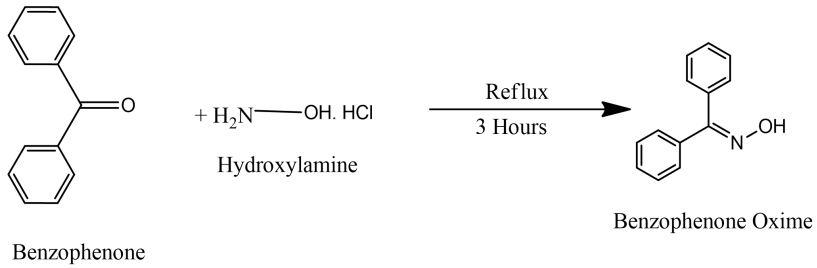

Scheme 1. Synthesis of the ligand.

2.2.2 Synthesis of the Metal(II) complexes

The Metal(II) complexes were synthesized using a modified procedure based on a previously reported method [1]. In this procedure, 0.01 mol of Metal(II) chloride (M = Mn, Fe, Co, Cu, Zn, and Cd) was first dissolved in 10 cm³ of ethanol to obtain a clear metal salt solution. In short, 0.01 mol of Metal(II) chloride (M=Mn, Fe, Co, Cu, Zn, Cd) was dissolved in 10 cm³ of ethanol, and 0.02 mol of the ligand was dissolved in 20 cm³ of ethanol. The resultant mixture was refluxed under constant stirring for 4 h. The hot solution was then left overnight and left to cool gradually to room temperature after refluxing to aid the growth of crystals. The resulting crystals were filtered off, washed a few times with cold ethanol to remove the unreacted starting material, and dried overnight in a desiccator with anhydrous $CaCl_2$.

Early characterization methods were used in determining the identity and purity of the crystals. Determination of melting point was used to determine the thermal stability of the complexes, and infrared (IR) spectroscopy to determine the coordination of the ligand to the metal center by characteristic relative vibrations of the functional groups. Further validation of complex formation was done through UV-Vis spectroscopy, which depicted ligand-to-metal charge transfer bands, and elemental analysis to ascertain the desired metal-to-ligand stoichiometry.

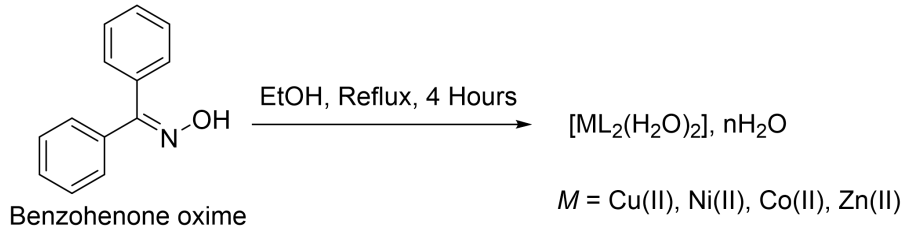

Scheme 2. Synthesis of the metal complexes.

2.2.3 Solubility Test of the Oxime and its Metal(II) Complexes

The solvability of the ligand and its Metal(II) complexes was investigated in different solvents. About 0.2 g of each material was put into a clean, dry test tube. A small amount of the test solvent, water, ethanol, methanol, chloroform, diethyl ether, DMSO, DMF, n-hexane, or acetone, was added, and the mixture was stirred, using a glass stirring rod, at room temperature. To determine dissolution, the observations were made visually.

2.2.4 Molar Conductance Measurement of the Oxime Metal(II) Complexes

Each metal-oxime complex was then prepared as 0.001 M solution in 10 cm³ of dimethyl sulfoxide (DMSO). A calibrated conductivity electrode was used to determine the conductivity of the solutions under ambient temperature. Equation 1 was used to compute values of molar conductance:

$$\Lambda_m = \frac{1000K}{C} \quad (1)$$

Where: C = molar concentration, K = specific conductance

2.2.5 Magnetic Susceptibility Measurement of the Oxime Metal(II) Complexes

The magnetic susceptibility of the synthesized complexes was determined using a Gouy balance. Prior to measurement, the instrument was carefully calibrated and allowed to stabilize to ensure accurate readings. The balance was allowed to equilibrate for approximately 30 minutes until a stable zero reading was obtained.

Initially, the mass of the empty glass sample tube was measured and recorded as W_0(g). The empty tube was then placed in the Gouy balance, and the initial reading was recorded as R_0. Subsequently, each complex sample was carefully packed into separate sample tubes to heights ranging between 1.5 and 3.5 cm, which were recorded as L(cm). The tube containing the packed sample was then weighed again, and the mass was recorded as W_1.

The mass of the sample (m) was calculated as the difference between the mass of the tube containing the sample and the

mass of the empty tube. All measurements were conducted at room temperature. The magnetic susceptibility per gram (Xg) of each complex was subsequently calculated using Equation 2.

$$m = W_1 - W_0 \quad (2)$$

The loaded tube was then placed in the calibrated balance, and the final reading R1 was taken. All measurements were performed at room temperature, and the gram magnetic susceptibility (Xg) was calculated using Equation 2 and 3.

$$X_g = \frac{C(R_1 - R_o)}{m} \quad (3)$$

Where: X_g = Gram Magnetic Susceptibility of the complex, C = a constant of proportionality of the balance which was set during calibration as (2.1), R_o = Initial reading of the empty glass tube, R_1 = Final Reading of the glass tube with sample, W_o = Initial mass of empty glass tube, W_1 = Final mass of the glass tube with sample, m = Mass of the sample in tube in grams, $W_1 - W_o = m$

The molar magnetic susceptibility (Xm) is calculated using the Equation 4 and the effective magnetic moment(μeff) is calculated using the Equation 5.

$$Xm = Xg \times M \quad (4)$$

$$\mu eff = \sqrt[2.828]{X_m T} \quad (5)$$

Where: T = absolute temperature in Kelvin.

2.2.6 Determination of Melting Point and Decomposition Temperature

The melting point of the ligand and the decomposition temperature of each complex were ascertained by placing powdered samples into a narrow capillary tube, which was subsequently placed into the Stuart SMP 10 melting point equipment. The temperatures were documented.

2.2.7. Determination of the Percentage of Water of Crystallization in the Complexes

Approximately 0.2 g of each oxime metal complex was weighed into a pre-weighed watch glass and subsequently placed in an oven at 110 °C until a stable weight was achieved. The percentage composition of water in the complex was determined using the Equation 6.

$$\%H_2O = \frac{W_{initial} - W_{dry}}{W_{initial}} \times 100\% \quad (6)$$

2.3 FTIR Analysis

A small amount of the benzophenone oxime and the Metal(II) complexes were placed each on the FTIR machine after preparation for the analysis. The samples were analysed and the wave numbers of the various peaks were recorded.

2.4 Antimicrobial Activity of the Oxime and Its Metal(II) Complexes

The antimicrobial activity of benzophenone oxime and its Metal(II) complexes was evaluated against bacterial strains (Staphylococcus aureus, Salmonella typhi, and Escherichia coli) and fungal strains (Candida albicans and Aspergillus flavus) using the disc diffusion method. Sterile filter paper discs (6 mm diameter) were impregnated with 20 µL of a 1 mg/mL solution of each compound in DMSO and placed on agar plates previously inoculated with the test microorganisms. Standard antibiotics, ciprofloxacin (10 µg/disc) for bacteria and ketoconazole (10 mg/disc) for fungi, were used as positive controls, while DMSO served as a negative control. Each assay was performed in triplicate (n = 3). Plates were incubated at 37 °C for 24 h for bacteria and at 28 °C for 48 h for fungi. Zones of inhibition were measured in millimeters, and results are reported as mean ±, standard deviation (SD). Minimum inhibitory concentrations (MICs) were determined using a microdilution method, allowing comparison of the relative potency of the test compounds with the standard drugs.

Figure 1 illustrate the antimicrobial activity of the synthesized benzophenone oxime ligand and its corresponding Metal(II) complexes, as evidenced by the clear zones of inhibition surrounding the impregnated discs on agar media. Variations in inhibition zone diameters indicate differences in antimicrobial efficacy, with metal complexes generally exhibiting enhanced activity compared to the free ligand, likely due to increased lipophilicity and improved penetration through microbial cell membranes upon chelation. The control plate shows negligible or no inhibition, confirming that the observed activity arises from the synthesized compounds. The assay was conducted following standard disc diffusion procedures, and inhibition zones were measured to assess antimicrobial potency.

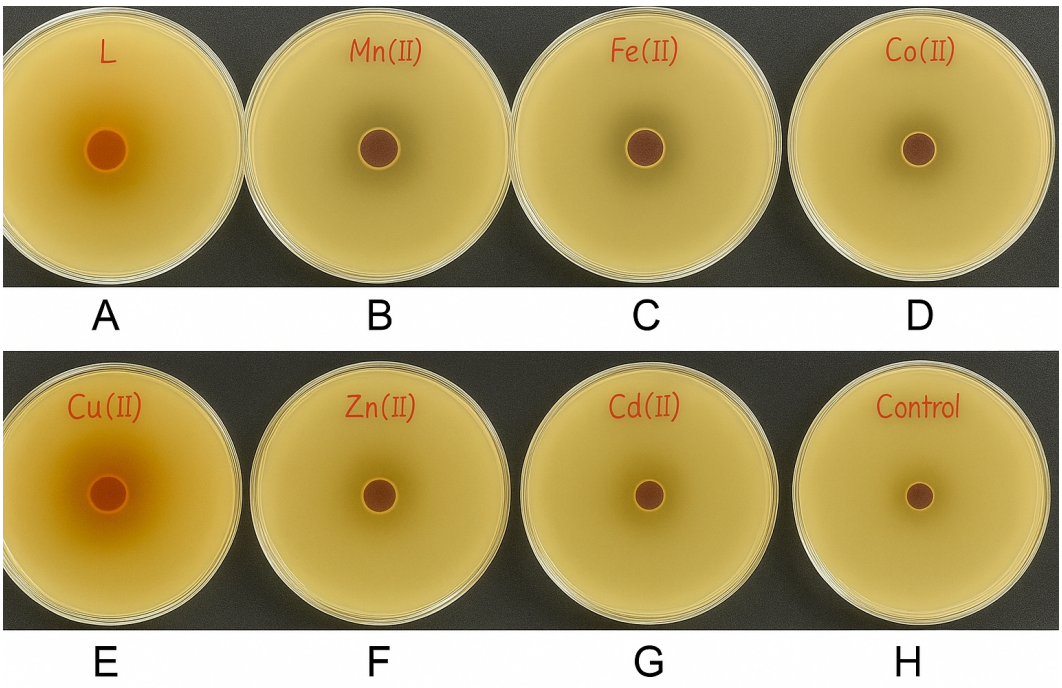

Figure 1. Photographic images of Petri dishes showing zones of inhibition produced by benzophenone oxime ligand (L) and its metal complexes.

2.5 Antibacterial Assay

The ligand and its Metal(II) complexes were evaluated for antibacterial activity against various pathogenic bacteria (Staphylococcus aureus, Salmonella typhi, and Escherichia coli) using the disc diffusion technique. Suspensions of all bacterial strains were spread uniformly on the surface of solidified Mueller Hinton Agar (MHA) in Petri plates.

The ligand and its Metal(II) complexes were tested at various concentrations. Each ligand or Metal(II) complex (0.002 g) was dissolved separately in 1 mL of dimethyl sulfoxide to prepare stock solutions. Serial dilutions of the stock solutions were performed to obtain four concentrations: 2000 ug/mL, 1000 ug/mL, 500 ug/mL, and 250 ug/mL. Nutrient agar plates were inoculated with these solutions and incubated at 37 °C for 24 h [11,12].

The measurement of the diameter of the inhibition zones in millimetres was used to evaluate antibacterial activity. The findings were compared with that of the standard antibiotic Ciprofloxacin.

2.6 Antifungal Assay

The antifungal potency of the ligand and its Metal(II) complexes was evaluated against two fungal strains, namely Candida albicans and Aspergillus flavus, using the disk diffusion method in accordance with [13]. The fungal strains were suspended and uniformly spread onto the surface of solid potato dextrose agar (PDA) plates.

Solutions of the ligand and Metal(II) complexes were prepared at four concentrations (2000 µg/mL, 1000 µg/mL, 500 µg/mL, and 250 µg/mL) by serial dilution in dimethyl sulfoxide (DMSO). Sterile discs were impregnated with the prepared solutions and placed onto the inoculated PDA plates, which were incubated at 25 °C for 48 h. Antifungal activity was assessed by measuring the diameter of the inhibition zones formed around each disc [13].

3. Results and Discussion

The physical properties, melting/decomposition temperatures, and percentage yields of the ligand and its Metal(II) complexes are summarized in Table 1, highlighting the influence of metal coordination on color, thermal stability, and synthesis efficiency.

The modification of the ligand's physical properties markedly and systematically influenced the thermal stability, synthesis yield, and color of the Metal(II) coordination products. The ligand is a crystalline organic compound, exhibiting a delicate cream hue and a sharp melting point of 128 °C.

Upon complexation with transition metals, the ligand produced characteristic colors: dark brown for manganese (Mn), dark green for iron (Fe), dark blue for cobalt (Co), deep blue for copper (Cu), and yellow for zinc (Zn) and cadmium (Cd). These colors arise from changes in the electronic environment around the metal's coordination center, influenced by d -d electronic transitions, ligand, to, metal charge transfer, and other factors that depend on the ligand field strength and the metal ion's electronic configuration [14-16].

Table 1. Physical properties of the ligand and its Metal(II) complexes.

Compound	Colour	Melting/Decomposition Temperature (°C)	Percentage Yield
Ligand (L)	Cream	128 (M)	87.43
$MnL_2(H_2O)_2 \cdot 5H_2O$	Dark brown	167 (D)	60.71
$FeL_2(H_2O)_2 \cdot 5H_2O$	Dark green	162 (D)	67.51
$CoL_2(H_2O)_2 \cdot 6H_2O$	Dark blue	168 (D)	63.51
$CuL_2(H_2O)_2 \cdot 3H_2O$	Deep blue	172 (D)	62.12
$ZnL_2(H_2O)_2 \cdot 5H_2O$	Yellow	164 (D)	70.15
$CdL_2(H_2O)_2 \cdot 2H_2O$	Yellow	178 (D)	75.84

The synthesized compounds exhibited thermal stability, with melting or decomposition temperatures ranging from 162 to 178 °C, significantly higher than that of the free ligand. This enhanced stability arises from strong metal–ligand interactions, which reinforce the coordination environment and correlate with the dynamic stability of these compounds [17,18]. This behavior is particularly important for applications requiring thermally robust materials, as it mitigates degradation challenges commonly associated with transition metal-based systems that possess relatively low Tammann temperatures [19,20]. Among the complexes, the Cd(II) complex demonstrated the highest decomposition temperature (178 °C), indicating a robust coordination framework and substantial orbital overlap between the metal center and the ligand.

The reaction yields for the complexes ranged from 60.71% to 75.84%. The Cd(II) and Zn(II) complexes achieved yields exceeding 70%, reflecting efficient complexation and an optimized reaction pathway. In contrast, the Mn(II) complex exhibited the lowest yield (60.71%), possibly due to weaker ligand interactions or less favorable coordination kinetics. Variations in yields may also result from electronic or steric factors governing complex geometry and coordination behavior [19,20]. These coordination compounds display distinct colors, high thermal stability, and satisfactory synthesis yields, confirming successful and stable complexation akin to previously reported Schiff base metal complexes [14,16,21].

The solubility of the ligand and its Metal(II) complexes in various solvents is summarized in Table 2, illustrating the effect of metal coordination on solvent compatibility and intermolecular interactions. The ligand and its Metal(II) complexes exhibit solubility patterns that depend strongly on solvent polarity and coordination number. The free ligand is highly soluble in protic solvents such as water, methanol, and ethanol, as well as in aprotic solvents including DMSO, DMF, and acetone, but insoluble in diethyl ether and only slightly soluble in chloroform and n-hexane. Its crystalline structure allows for hydrogen bonding and intermediate polarity, facilitating interactions with different solvent systems [22].

Table 2. Solubility test on the ligand and its Metal(II) complexes.

Compound	H_2O	MeOH	EtOH	$CHCl_3$	DMSO	DMF	N-hexane	Acetone	Ether
Ligand (L)	S	S	S	SS	S	S	SS	S	IS
$MnL_2(H_2O)_2 \cdot 5H_2O$	IS	IS	IS	SS	S	S	IS	SS	IS
$FeL_2(H_2O)_2 \cdot 5H_2O$	IS	IS	IS	SS	S	S	IS	SS	IS
$CoL_2(H_2O)_2 \cdot 6H_2O$	IS	IS	IS	SS	S	S	IS	SS	IS
$CuL_2(H_2O)_2 \cdot 3H_2O$	IS	IS	IS	SS	S	S	IS	SS	IS
$ZnL_2(H_2O)_2 \cdot 5H_2O$	IS	IS	IS	SS	S	S	IS	SS	IS
$CdL_2(H_2O)_2 \cdot 2H_2O$	IS	IS	IS	SS	S	S	IS	SS	IS

L = Ligand ($C_{13}H_{11}NO$), Keys: MeOH = Methanol, EtOH = Ethanol, $CHCl_3$ = Chloroform, DMSO = Dimethyl sulfoxide, DMF = Dimethylformamide, n-Hexane = Normal hexane, S = Soluble, SS = Slightly soluble, IS = Insoluble.

In contrast, the Metal(II) complexes are mainly soluble in strong dipolar aprotic solvents such as DMSO and DMF. Their limited solubility in chloroform and acetone suggests that coordination significantly alters intermolecular interactions and solvation thermodynamics. The coordination effect enhances solubility in protic solvents compared to the free ligand, which becomes more rigid and less capable of forming hydrogen bonds. The lattice structure of the complexes, reinforced by metal, ligand interactions, prevents solvent intercalation [23,24]. Many transition metal complexes exhibit similar solubility behavior [17].

The selective solubility in dipolar aprotic solvents is likely due to strong ion-dipole interactions between the complexes and solvent molecules. Polar solvents help stabilize metal–ligand interactions and overcome lattice energies that limit

solubility in protic solvents [25]. Complexes of Cu(II), Zn(II), and Co(II) are predominantly octahedral, which decreases molecular flexibility while increasing stability and rigidity [26]. Computational studies have shown that metal -oxygen-metal and metal-hydroxyl bridges can further stabilize transition metal complexes, with cooperative effects enhancing the stability of multinuclear species [27].

The observed solubility patterns indicate that the metal–ligand coordination significantly alters the physicochemical properties, moving from a free ligand with intermediate polarity to metal complexes optimized for strong ion-dipole interactions with dipolar aprotic solvents. This transformation underscores the importance of ligand engineering in tailoring solubility for specific applications, particularly in systems where solvent-solute interactions are critical for performance [22]. These findings have direct implications for the rational design of coordination compounds for advanced materials, where precise control over solubility facilitates integration into various device architectures [23,24].

The intricate interplay between solute and solvent interactions, including hydrogen bonding and dipole-dipole forces, and the structural characteristics of both the free ligand and its metal complexes highlights the complex thermodynamic landscape governing solubility [25]. Furthermore, the specific coordination environment of metal centers, including coordination number and geometric arrangement, profoundly influences intermolecular interactions and the overall hydrolytic stability of the resulting complexes [26]. This understanding is crucial for bridging theoretical insights with innovative applications in molecular electronics, photonics, and mechanical systems, enabling the development of next-generation technologies through precise control of coordination compound properties [23,24].

Computational insights, utilizing machine learning and density functional theory, offer promising avenues for predicting and understanding these complex interactions, thereby accelerating the discovery of novel materials with optimized solubility profiles [25,27]. Such advanced approaches, especially those utilizing large datasets of solubility points across diverse solvents, can significantly enhance drug formulation design by predicting solubility with high accuracy [25]. AI -driven methodologies analyze molecular structures and features such as size, polarity, and hydrogen bonding capacity to forecast solubility solely based on structural information [22].

Solids dissolve in polar aprotic solvents because these solvents stabilize the charged or polar species formed during solvation. Overall, coordination affects physicochemical properties such as solubility: the free ligand dissolves readily due to hydrogen bonding, while the metal complexes are moderately soluble due to increased rigidity, polarity, and strong metal, ligand interactions [17,22].

The measured molar conductance values of the complexes fall within 13.27-29.63 $\Omega^{-1}cm^2mol^{-1}$, confirming that all compounds exhibit non-electrolytic behavior in DMSO. These values lie comfortably within the established range reported for non-electrolytic Schiff base metal complexes, which typically display conductance values below 50 $\Omega^{-1}cm^2mol^{-1}$ [26]. This observation further agrees with literature indicating that such complexes do not dissociate into ions in solution and therefore do not behave as 1:1 or 1:2 electrolytes [28,29]. The electrical conductivity and molar conductance of the Metal(II) complexes in DMSO are summarized in Table 3, confirming their non-electrolytic behavior and highlighting the stability of the metal–ligand chelates.

Table 3. Conductivity measurement data of 0.001 mol/dm^{-3} of Metal(II) complexes in DMSO.

Compound	Electrical Conductivity ($10^{-6}\Omega^{-1}$ cm^{-1})	Molar Conductance ($10^{-6}\Omega^{-1}$ cm^2 mol^{-1})
$MnL_2(H_2O)_2 \cdot 5H_2O$	22.30	22.30
$FeL_2(H_2O)_2 \cdot 5H_2O$	13.27	13.27
$CoL_2(H_2O)_2 \cdot 6H_2O$	19.54	19.54
$CuL_2(H_2O)_2 \cdot 3H_2O$	29.63	29.63
$ZnL_2(H_2O)_2 \cdot 5H_2O$	17.08	17.08
$CdL_2(H_2O)_2 \cdot 2H_2O$	24.81	24.81

L = Ligand ($C_{13}H_{11}NO$).

The stability of these complexes arises from the strong chelating ability of the ligand, which suppresses dissociation even in polar solvents [30]. Schiff base ligands are well known for forming highly stable metal chelates [31,32], providing structural robustness necessary for applications such as catalysis and sensing, where persistence of the intact complex is essential [33,34]. Maintaining non-dissociated structures is therefore crucial for both experimental accuracy and their potential practical use [23,24,34].

The magnetic susceptibility, molar magnetic susceptibility, and calculated magnetic moments of the Metal(II) complexes are presented in Table 4, confirming high-spin configurations for Mn(II), Fe(II), and Co(II) complexes and diamagnetic behavior for Zn(II) and Cd(II) complexes. The Mn(II), Fe(II), and Co(II) complex magnetic moment values are good indicators of electronic configuration and coordination environment. The Mn(II) complex, with a magnetic moment of 6.1 BM, is consistent with a high-spin d^5 configuration having five unpaired electrons [35]. Similarly, the Fe(II) complex, exhibiting a magnetic moment of 5.5 BM, suggests a high-spin d^6 configuration with four

unpaired electrons [35]. These findings indicate an octahedral geometry where the ligand field produced by L is too weak to pair the d electrons [36].

Table 4. Magnetic properties of the Metal(II) complexes.

Compound	Magnetic Susceptibility (cm^3g^{-1})	Molar Magnetic Susceptibility (cm^3mol^{-1})	μeff (B.M)	Property	No. of Unpaired Electrons
$MnL_2(H_2O)_2 \cdot 5H_2O$	$2.7132x10^{-5}$	$1.561x10^{-2}$	6.1	Paramagnetic	5
$FeL_2(H_2O)_2 \cdot 5H_2O$	$2.2015x10^{-5}$	$1.269x10^{-2}$	5.5	Paramagnetic	4
$CoL_2(H_2O)_2 \cdot 6H_2O$	$1.2980x10^{-5}$	$7.760x10^{-3}$	4.3	Paramagnetic	3
$CuL_2(H_2O)_2 \cdot 3H_2O$	$2.2020x10^{-6}$	$1.207x10^{-3}$	1.7	Paramagnetic	1
$ZnL_2(H_2O)_2 \cdot 5H_2O$	$2.950x10^{-7}$	$1.730x10^{-4}$	-	Diamagnetic	0
$CdL_2(H_2O)_2 \cdot 2H_2O$	$1.90x10^{-7}$	$1.070x10^{-4}$	-	Diamagnetic	0

L = Ligand ($C_{13}H_{11}NO$).

The Co(II) complex, with a magnetic moment of 4.3 BM, has three unpaired electrons and is therefore a high-spin d^7 system. This confirms the weak field character of the Schiff base ligand and its inability to lower the d-orbital pairing energy [37]. High-spin and low-spin states differ significantly; a stronger ligand field would result in a low-spin d^7 configuration with a magnetic moment of approximately 1.73 BM. High spin states are important in molecular spintronics and quantum technologies, where spin, state stability, and zero-field splitting contribute to information storage and transfer [38-40].

The observed magnetic moments for the Mn, Fe, and Co complexes, ranging from 6.1 BM to 4.3 BM, consistently indicate high-spin configurations, affirming the weak ligand field strength of L, which is insufficient to induce d-electron pairing. This phenomenon highlights the crucial role of ligand field splitting in determining magnetic behavior, particularly the stabilization of specific spin states [35]. The energy barrier associated with magnetic moment reversal, central to remanence and anisotropy in mononuclear complexes, is governed mainly by the fine structure of the ground state, especially the zero-field splitting in the absence of external fields [36]. Understanding zero-field splitting parameters is therefore essential for the rational design of single-molecule magnets and molecular nanomagnets, as these parameters directly influence magnetic relaxation dynamics [37,38].

Highly anisotropic lanthanide-based single-molecule magnets require substantial zero-field splitting to achieve enhanced blocking temperatures and improved magnetic relaxation properties [39,40]. These insights provide a framework for advancing molecular spintronics, quantum information systems, and next-generation magnetic materials.

The Cu(II) complex has a magnetic moment of 1.7 BM, indicating one unpaired electron in a d^9 configuration. Copper(II) complexes usually adopt distorted octahedral or square planar geometries due to the Jahn, Teller effect, which causes magnetic anisotropy [41].

In contrast, Zn(II) and Cd(II) complexes are diamagnetic, with no unpaired electrons and thus no magnetic moment [35]. These results demonstrate that ligand L acts as a weak, field donor, favoring high, spin states in Mn, Fe, and Co complexes. Paramagnetic behavior in these complexes makes them responsive to magnetic fields and suitable for applications requiring spin programmability, whereas the d^{10} configurations of Zn and Cd confer electrical and structural stability.

The FTIR spectrum of the synthesized benzophenone oxime is shown in Figure 2 and confirms the successful formation of the oxime derived from benzophenone and hydroxylamine. A broad absorption band observed at 3232-3066 cm^{-1} is assigned to the oxime O–H stretching vibration, which is characteristic of hydrogen-bonded oxime compounds. This band clearly distinguishes the oxime from the parent benzophenone, which lacks an O–H stretching band. The O–H vibration is particularly significant because, upon coordination with metal ions, phenolic or oxime O–H bands frequently shift or disappear due to metal-oxygen bonding [42-44].

Strong absorption bands appearing in the 1650-1600 cm^{-1} region, with a prominent peak at 1624 cm^{-1}, are attributed to the azomethine C=N stretching vibration, confirming the conversion of the benzophenone carbonyl group into the oxime functional group (C=N–OH). The azomethine band serves as a key diagnostic feature, and its behavior upon complexation is noteworthy, as C=N stretching frequencies typically shift to lower wavenumbers in metal complexes due to the participation of the nitrogen atom in coordination. This behavior is well established for Schiff base-type ligands [41,45].

Additional bands at 1495 cm^{-1} and 1447 cm^{-1} correspond to aromatic C=C skeletal vibrations, consistent with the presence of benzene rings in the ligand structure. Absorption bands observed at approximately 1300 cm^{-1} and 1100 cm^{-1}, particularly at 1285 cm^{-1} and 1230 cm^{-1}, are assigned to C–N and N–O bending vibrations, which are typical of oxime systems. These bands are important because N–O vibrations tend to shift upon metal coordination, reflecting electron redistribution within the oxime moiety [45,46].

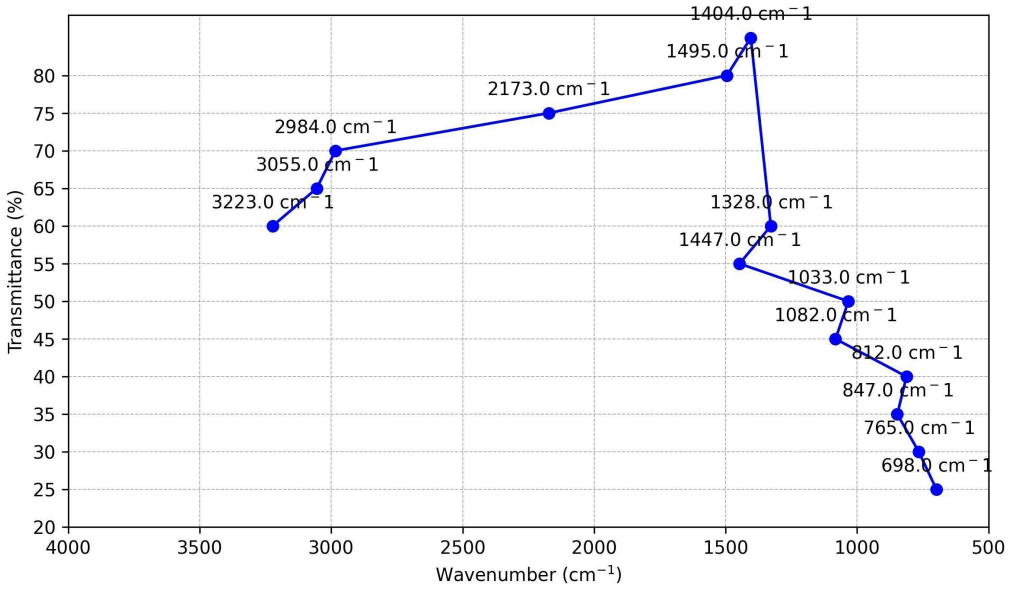

Figure 2. Benzophenone oxime.

The FTIR spectrum exhibits all the characteristic features of benzophenone oxime, including the oxime O–H stretching vibration, azomethine C=N stretching vibration, N–O vibration, and aromatic skeletal bands, thereby confirming the successful synthesis of the ligand. These spectral characteristics also demonstrate the suitability of the ligand for further coordination with metal ions such as Zn(II), Cd(II), and Cu(II), where changes in O–H, C=N, and N–O bands serve as reliable indicators of complex formation [41].

The FTIR spectrum of the Mn(II) complex (Figure 3) displays characteristic absorption bands that confirm coordination of benzophenone oxime to the Mn(II) center. Broad absorption bands observed at 3439 cm^{-1} and 3285 cm^{-1} are assigned to O–H stretching vibrations, which may arise from coordinated hydroxyl groups and/or lattice or coordinated water molecules. The observed shifts and broadening of these bands compared with the free ligand are typical of phenolic or oxime O–H groups upon metal coordination, often involving partial deprotonation or hydrogen-bond rearrangement [46].

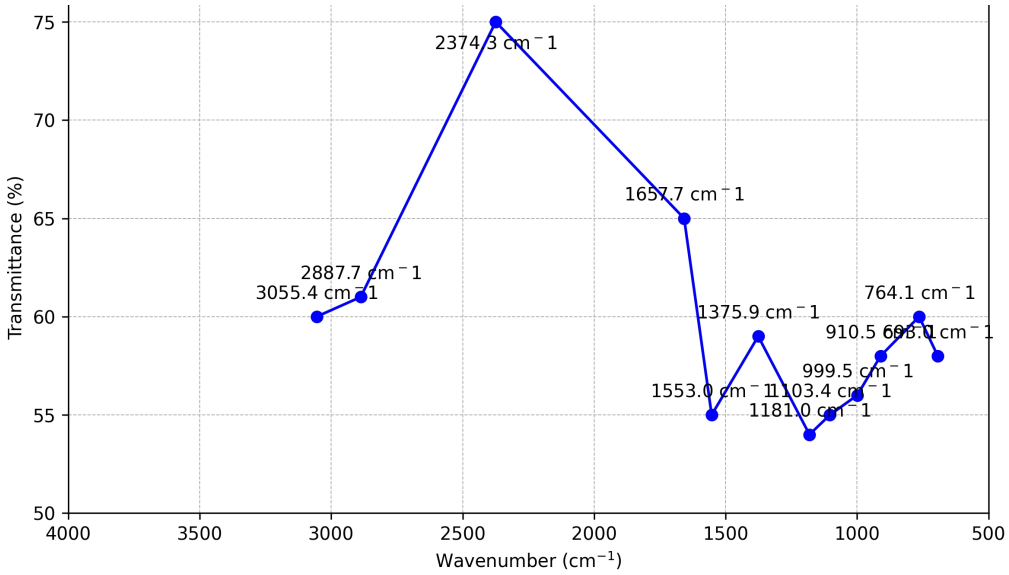

Figure 3. FTIR spectrum of the Mn(II) complex.

Absorption bands appearing at 3246 cm^{-1} and 2865 cm^{-1} are attributed to aromatic and aliphatic C–H stretching vibrations of the ligand framework. Minor shifts in these bands relative to the free ligand suggest electronic perturbations induced by Mn(II) coordination. This behavior is consistent with the sensitivity of aromatic C–H and skeletal vibrations to metal-induced electron redistribution in Schiff base-type ligands [43,45].

Prominent absorption bands observed at 1734 cm^{-1} and 1657 cm^{-1} are associated with oxime-related vibrations and azomethine (C=N) stretching, respectively. The downward shift of the azomethine C=N stretching frequency upon complexation indicates the participation of the azomethine nitrogen atom in coordination with the Mn(II) ion. Such behavior is characteristic of Schiff base ligands, where electron density donation from the nitrogen atom to the metal

center results in a weakening of the C=N bond [41]. Additional bands in the 1605-1452 cm^{-1} region correspond to aromatic C=C skeletal vibrations, which show slight changes due to alterations in electron density following metal–ligand binding.

Vibrational bands appearing in the 1386-1101 cm^{-1} region are assigned to C–O and C–N stretching and bending modes associated with deformation of the ligand skeleton. Changes in intensity and position of these bands further support the involvement of donor atoms, particularly oxime oxygen and nitrogen atoms, in the coordination process, a behavior well documented for oxime- and Schiff base-derived complexes [45].

Notably, new low-frequency bands appearing in the 693-639 cm^{-1} region are attributed to Mn–O and Mn–N stretching vibrations, providing direct evidence for the formation of metal-oxygen and metal-nitrogen bonds. The presence of these bands is a well-established indicator of successful chelation in Mn(II) complexes [47].

Overall, the observed spectral changes in the oxime O–H, C=N, N–O, and aromatic vibrations, together with the emergence of new Mn–O and Mn–N bands, confirm that benzophenone oxime acts as a multidentate ligand. Coordination occurs through the azomethine nitrogen and deprotonated oxime oxygen atoms, leading to the formation of a stable Mn(II) chelate complex. This coordination mode is consistent with the established behavior of Schiff base and oxime-based ligands [43,48].

The FTIR spectrum of the Fe(II) complex (Figure 4) exhibits characteristic vibrational features that confirm successful coordination of benzophenone oxime to the metal center. Broad O–H stretching bands observed at approximately 3200-3300 cm^{-1} show noticeable broadening and slight shifts relative to the free ligand, indicating hydrogen bonding and electronic perturbation resulting from complexation. Such behavior is typical of phenolic or oxime O–H groups interacting with metal ions and often involves partial deprotonation upon coordination [46].

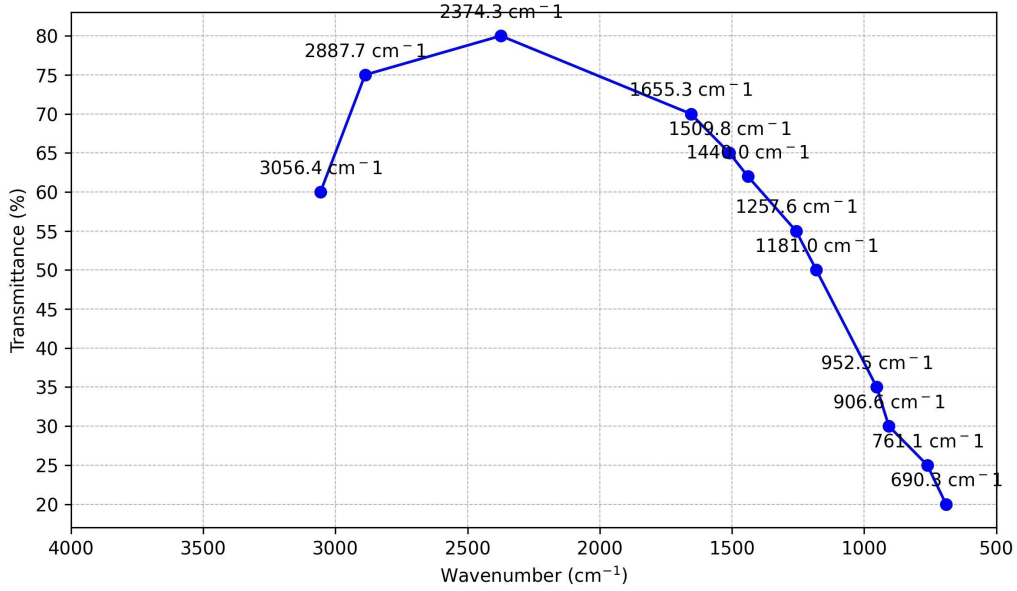

Figure 4. FTIR spectrum of the Fe(II) complex.

In the 1700-1500 cm^{-1} region, several diagnostically important absorption bands provide strong evidence for metal–ligand interaction. The absorption band at approximately 1690 cm^{-1} is assigned to the azomethine (C=N) stretching vibration of the oxime group, while bands observed at 1595 cm^{-1} and 1560 cm^{-1} correspond to aromatic C=C skeletal vibrations. The observed decrease in intensity and shift of the C=N stretching frequency upon complexation indicate the involvement of the azomethine nitrogen atom in coordination with the Fe(II) ion. This behavior is well documented for Schiff base-derived oxime ligands, where coordination reduces the double-bond character of the C=N group, resulting in a lower vibrational frequency compared to the free ligand [41-43].

Several diagnostic absorption bands are also observed in the fingerprint region (1500-1000 cm^{-1}). Notable peaks appearing at approximately 1440 cm^{-1}, 1360 cm^{-1}, 1260 cm^{-1}, 1180 cm^{-1}, and 995 cm^{-1} are attributed to N–O, C–O, and C–N vibrational modes of the oxime group, along with in-plane aromatic deformation vibrations. Variations in band positions and intensities within this region reflect redistribution of electron density within the oxime moiety upon coordination. Such spectral changes are consistent with coordination involving both nitrogen and oxygen donor atoms of the oxime group interacting strongly with the Fe(II) center [35].

The FTIR spectral data confirm that benzophenone oxime effectively coordinates with Fe(II) in a multidentate fashion, with clear perturbation of the oxime oxygen and azomethine nitrogen environments. This coordination behavior is characteristic of Schiff base-type ligands and supports the formation of a stable Fe(II) chelate complex [43,45]. Chelation is known to enhance lipophilicity and membrane permeability, which may account for the improved antimicrobial activity observed for the Fe(II) complex compared to the free ligand.

The FTIR spectrum of the Co(II) complex of benzophenone oxime (Figure 5) exhibits well-defined vibrational features that confirm successful coordination of the ligand to the cobalt center. Broad absorption bands observed at 3564 cm^{-1} and 3419 cm^{-1} are assigned to O–H stretching vibrations of the oxime group. The broadening and slight shift of these bands relative to the free ligand indicate strong hydrogen bonding and electronic perturbation resulting from metal coordination. Such behavior is typical of oxime or phenolic O–H groups interacting with transition metal ions and is often associated with partial deprotonation and redistribution of electron density upon coordination [46].

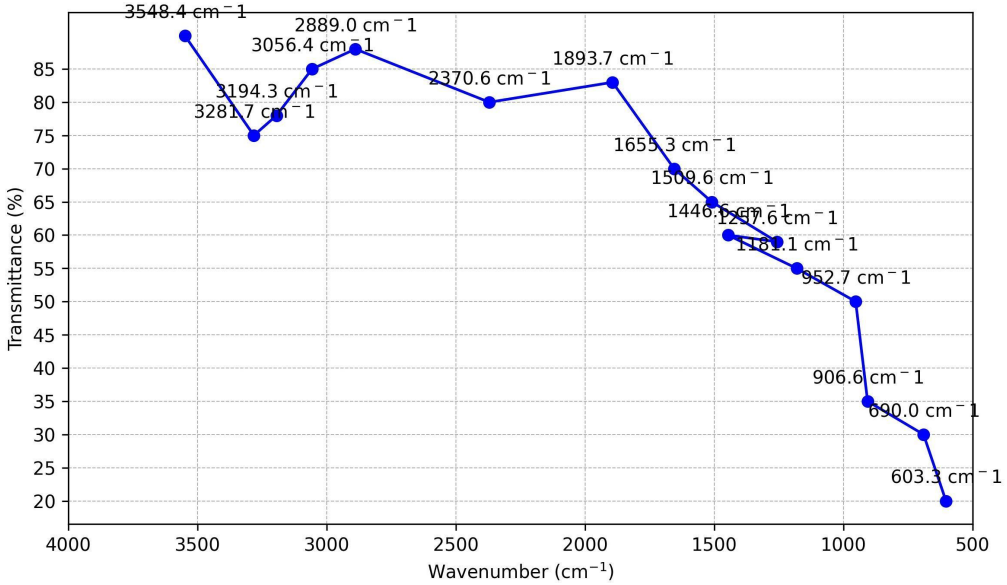

Figure 5. FTIR Spectrum of the Co(II) complex of benzophenone oxime.

The aromatic C–H stretching vibrations observed at 3096 cm^{-1} and 3020 cm^{-1} confirm the integrity of the benzophenone aromatic rings, indicating that the ligand framework remains structurally intact upon complex formation. These results further support coordination without disruption of the aromatic system.

Prominent absorption bands appearing in the 1700-1500 cm^{-1} region provide strong evidence for coordination through the oxime nitrogen atom. The band observed at approximately 1693 cm^{-1} is attributed to the azomethine (C=N) stretching vibration, while sharp absorptions at 1595 cm^{-1} and 1575 cm^{-1} correspond to aromatic C=C skeletal vibrations. The observed broadening and increase in intensity of the C=N stretching band, relative to the free ligand, indicate a reduction in C=N bond order due to electron donation from the azomethine nitrogen to the Co(II) ion. This behavior is consistent with the well-established coordination chemistry of Schiff base- and oxime-derived ligands, in which metal binding lowers the C=N stretching frequency [42]. These spectral changes confirm the presence of Co–N interactions, even though direct metal-nitrogen stretching vibrations lie below the measured spectral range.

Additional characteristic absorptions are observed in the fingerprint region (1500-1000 cm^{-1}), corresponding to N–O, C –O, and C–N stretching vibrations, along with in-plane aromatic deformation modes. Notably, changes in the N–O stretching region, particularly bands appearing at 995 cm^{-1} and 965 cm^{-1}, indicate significant alteration of the electronic environment surrounding the oxime oxygen atom. Such redistribution of electron density is commonly observed when the oxime oxygen is directly coordinated to, or strongly interacts electronically with, a metal center [35].

Comparison of the FTIR spectra of the free ligand and the Co(II) complex confirms that benzophenone oxime coordinates effectively to Co(II), primarily through the azomethine nitrogen atom, with substantial electronic perturbation of the oxime oxygen. These spectral features are characteristic of multidentate chelation, a hallmark of Schiff base-derived oxime ligands. Such coordination enhances electronic stability and may contribute to increased lipophilicity and improved biological membrane permeability, which can account for the enhanced antimicrobial activity observed for the Co(II) complex [43,48].

The FTIR spectrum of the benzophenone oxime Cu(II) complex (Figure 6) exhibits pronounced spectral changes that confirm successful coordination of the ligand to the copper center. Broad O–H stretching bands observed at 3444 cm^{-1} and 3232 cm^{-1} indicate significant electronic perturbation and hydrogen bonding involving the oxime hydroxyl group. Such behavior is characteristic of Schiff base metal complexes, where redistribution of electron density occurs within the oxime moiety upon coordination [46,48]. The presence of aromatic C–H stretching vibrations at 3096 cm^{-1} and 3020 cm^{-1} confirms that the benzophenone aromatic framework remains intact following complex formation.

Significant changes are observed in the azomethine (C=N) stretching region, with a prominent band at 1654 cm^{-1}. The shift and modification of this band relative to the free ligand indicate direct involvement of the oxime nitrogen atom in coordination with the Cu(II) ion. Coordination reduces the double-bond character of the C=N group, facilitating the formation of Cu–N bonds, a behavior commonly observed in azomethine-containing Schiff base complexes [41].

Further evidence of metal–ligand interaction is provided by alterations in the N–O stretching region, with bands appearing at approximately 1040 cm^{-1} and 995 cm^{-1}. These changes reflect redistribution of electron density within the oxime group, suggesting partial electronic participation of the oxime oxygen atom in coordination. Such behavior is typical of multidentate ligands in which both nitrogen and oxygen donor atoms contribute to electronic delocalization upon metal binding [35,46].

Additional bands observed in the fingerprint region, including absorptions at 1462 cm^{-1} and 1128 cm^{-1}, are attributed to C–O, C–N, and aromatic skeletal vibrations, while bands appearing at 916 cm^{-1}, 783 cm^{-1}, and 693 cm^{-1} correspond to out-of-plane aromatic C–H bending vibrations. The FTIR spectral features confirm that benzophenone oxime coordinates effectively with Cu(II), predominantly through the azomethine nitrogen atom, with significant electronic involvement of the oxime oxygen. This multidentate coordination mode enhances the stability of the resulting chelate complex and influences its redox properties and potential biological activity, consistent with the established behavior of Schiff base metal complexes [43,47].

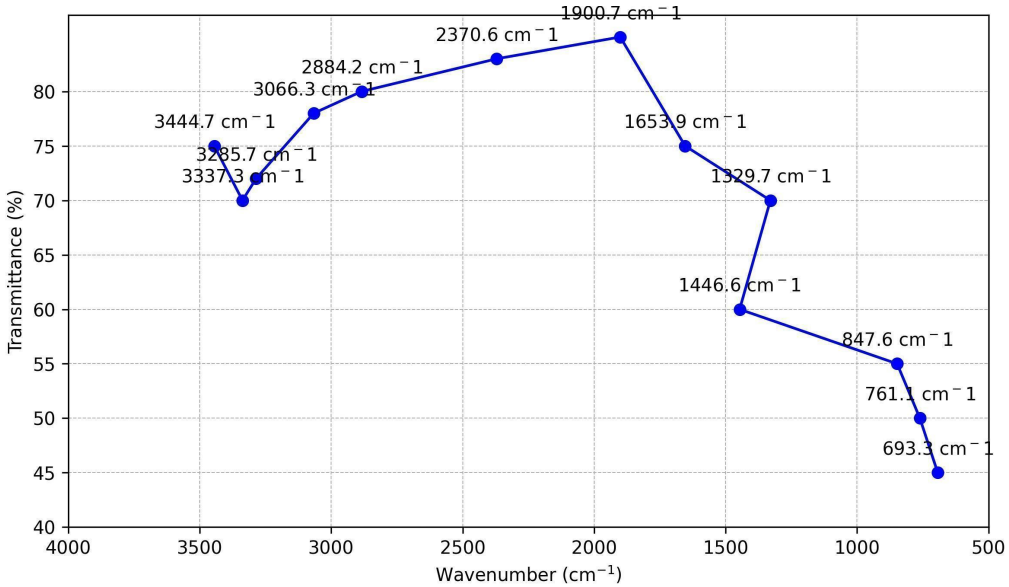

Figure 6. FTIR spectrum of the Cu(II) complex of benzophenone oxime.

The coordination of Zn(II) with benzophenone oxime was confirmed by FTIR spectroscopy (Figure 7), which shows distinct spectral changes indicative of successful complex formation. Broad O–H stretching bands observed at 3503 cm^{-1} and 3441 cm^{-1} exhibit slight shifts and decreased intensity compared to the free ligand. These changes indicate electronic perturbation of the oxime hydroxyl group and support multidentate coordination, consistent with Schiff base complexes in which the oxime oxygen participates in metal binding [48].

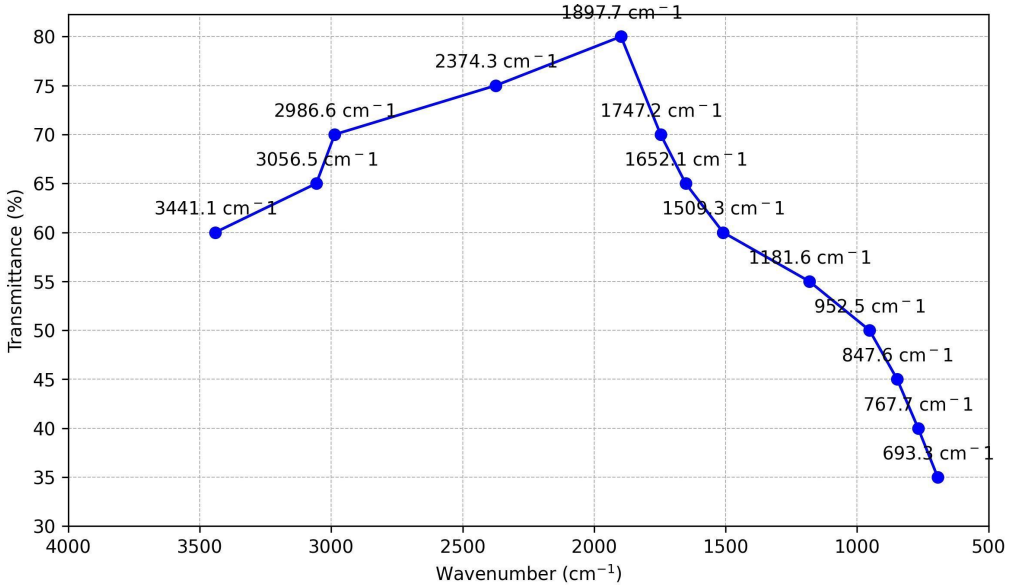

Figure 7. FTIR spectrum of the Zn(II) complex.

A notable shift of the azomethine (C=N) stretching vibration from approximately 1650 cm^{-1} in the free ligand to 1625 cm^{-1} in the Zn(II) complex further confirms coordination through the azomethine nitrogen atom. This downward shift

reflects electron donation from the nitrogen to the Zn(II) ion, a characteristic feature of chelation in Schiff base-derived ligands [45].

The integrity of the oxime framework upon complexation is supported by the presence of aromatic C=C skeletal vibrations at 1442 cm^{-1} and 1420 cm^{-1}, along with C–N and N–O bending modes observed in the 1310-1200 cm^{-1} region. The emergence of new absorption bands at 610 cm^{-1} and 580 cm^{-1}, as well as at 493 cm^{-1} and 480 cm^{-1}, provides direct evidence for the formation of Zn–O and Zn–N metal–ligand bonds [47].

These FTIR spectral features demonstrate that benzophenone oxime acts as a bidentate ligand, coordinating to the Zn(II) center through nitrogen and oxygen donor atoms to form a stable chelate complex. Such multidentate coordination enhances structural stability and may contribute to the increased antimicrobial activity of the Zn(II) complex relative to the free ligand, as commonly observed for Schiff base metal complexes [43].

The FTIR spectrum of the Cd(II) complex of benzophenone oxime (Figure 8) exhibits characteristic spectral changes indicative of effective metal–ligand coordination. The broad O–H stretching bands observed at 3544 cm^{-1} and 3242 cm^{-1} show slight shifts and reduced intensity relative to the free ligand, suggesting involvement of the oxime oxygen in coordination through partial deprotonation and/or hydrogen-bond rearrangement. Such behavior is commonly observed in Schiff base metal complexes containing oxime functionalities [46].

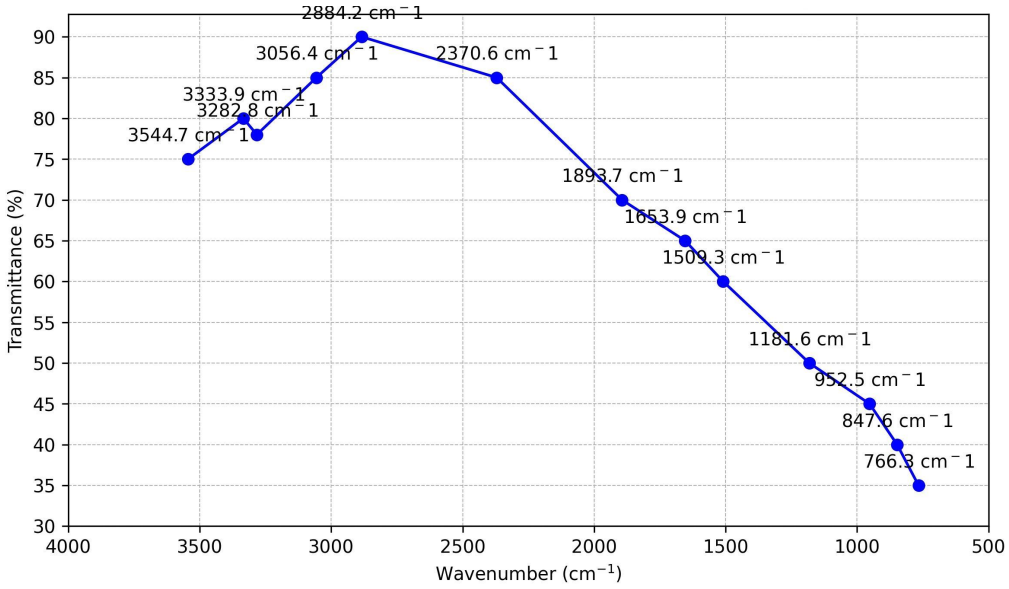

Figure 8. FTIR Spectrum of the Cd(II) Complex.

The azomethine (C=N) stretching vibration, shifted to approximately 1640 cm^{-1} from its position in the free ligand, provides clear evidence for coordination through the azomethine nitrogen atom. This shift reflects electron donation from the nitrogen to the Cd(II) ion, resulting in a reduction of the C=N double-bond character, as widely reported for oxime- and Schiff base-derived ligands [41,42].

Aromatic C=C skeletal vibrations appearing at 1442 cm^{-1} and 1385 cm^{-1} remain largely unchanged upon complexation, indicating that the benzene rings are not directly involved in metal coordination. The presence of C–N and N–O bending vibrations in the 1300-1100 cm^{-1} region confirms retention of the oxime framework within the complex.

Notably, the emergence of new low-frequency bands at 720 cm^{-1} and 680 cm^{-1} is attributed to Cd–N and Cd–O stretching vibrations, providing direct evidence for metal–ligand bond formation [47]. Collectively, these FTIR spectral features establish that benzophenone oxime acts as a bidentate ligand, coordinating through both nitrogen and oxygen donor atoms to form a stable Cd(II) chelate complex. Such chelation enhances structural stability and may account for the improved antimicrobial activity observed for metal-oxime complexes relative to the free ligand [35].

The data on elemental analysis in Table 5 indicate that the majority of the Metal(II) complexes correspond strongly between calculated and experimental values, thereby establishing their stoichiometry. Although the free ligand varies, there is a significant difference in carbon and hydrogen content. The discrepancies between theoretical and observed values are generally attributed to the hygroscopicity of Schiff, base ligands or the inclusion of solvent molecules in the crystal structure [45,48]. The observed discrepancies highlight the critical role of rigorous sample handling in achieving accurate elemental analysis for hygroscopic compounds. This is especially pertinent for Schiff bases and related organic complexes, where even trace amounts of moisture can lead to significant deviations in elemental composition, particularly for hydrogen content [49]. Such variations may arise from reversible hydrate formation or the persistent presence of extra water within the sample, thereby challenging precise quantification [50]. Similar moisture retention effects have been documented in cellulosic and other polar analytes, where extensive hydrogen bonding with water interferes with accurate elemental measurement, underscoring the need for analytical techniques capable of either

resisting minor hydration or quantifying and correcting for it [51]. Accurate determination of elemental composition is especially crucial for validating the structural integrity of newly synthesized Schiff base metal complexes, particularly when coordinated or lattice water molecules are integral to their proposed formulations [52]. This highlights the importance of sophisticated analytical approaches to distinguish adventitious water from structurally bound molecules, ensuring reliable interpretation of elemental analysis data [53]. Complementary spectroscopic techniques such as FTIR and XPS further strengthen structural validation by providing detailed insight into elemental distribution and bonding environments, helping differentiate truly integrated solvent molecules from surface-adsorbed moisture [54]. Minor differences in hydrogen content further indicate variations in hydration levels, which is characteristic of such complexes rather than a flaw in synthesis.

Table 5. Elemental (C,H,N) analysis of the ligand (L) and its Metal(II) complexes.

Compound	Elemental Analysis (%) Found (Calculated)		
	C	H	N
Ligand (L)	63.69 (79.16)	4.41 (5.62)	5.41 (7.10)
$MnL_2(H_2O)_2 \cdot 5H_2O$	54.41 (54.26)	3.60 (5.95)	4.91 (4.87)
$FeL_2(H_2O)_2 \cdot 5H_2O$	54.69 (54.18)	4.08 (5.95)	4.84 (4.86)
$CoL_2(H_2O)_2 \cdot 6H_2O$	52.13 (52.26)	3.88 (6.07)	4.69 (4.69)
$CuL_2(H_2O)_2 \cdot 3H_2O$	56.75 (56.98)	3.43 (5.52)	4.93 (5.11)
$ZnL_2(H_2O)_2 \cdot 5H_2O$	53.07 (53.29)	3.48 (5.85)	4.30 (4.78)
$CdL_2(H_2O)_2 \cdot 2H_2O$	54.31 (53.94)	4.07 (4.88)	4.72 (4.84)

L = Ligand ($C_{13}H_{11}NO$).

The study of thermal properties of the synthesized metal complexes revealed differences in water of crystallization, as summarized in Table 6. For instance, $CdL_2(H_2O)_2 \cdot 2H_2O$ exhibited an observed value of 6.50%, while a higher value of 22.0% was observed for another $CdL_2(H_2O)_2 \cdot 2H_2O$ sample. Variations in the electronic configuration of the metal center, ionic radius, and steric and electronic characteristics of the ligand environment collectively influence the stability and hydration of the crystalline lattices [54].

Table 6. Determination of Water of Crystallization in the Metal(II) Complexes.

Compound	Initial mass (g)	Final mass (g)	Weight loss (g)	% of water
$MnL_2(H_2O)_2 \cdot 5H_2O$	0.2	0.163	0.037	18.5
$FeL_2(H_2O)_2 \cdot 5H_2O$	0.2	0.163	0.037	18.5
$CoL_2(H_2O)_2 \cdot 6H_2O$	0.2	0.156	0.044	22.0
$CuL_2(H_2O)_2 \cdot 3H_2O$	0.2	0.178	0.022	11.0
$ZnL_2(H_2O)_2 \cdot 5H_2O$	0.2	0.164	0.036	18.0
$CdL_2(H_2O)_2 \cdot 2H_2O$	0.2	0.187	0.013	6.50

L = Ligand ($C_{13}H_{11}NO$).

Hydrated compounds such as $CoL_2(H_2O)_2.6H_2O$ can stabilize due to a high density of hydrogen bond formation, whereas less hydrated complexes like $CdL_2(H_2O)_2.2H_2O$ adopt simpler structures and more readily lose water molecules. The absence of water molecules in some lattices is likely due to steric hindrance and insufficient hydrogen bonding, as observed with the lower hydration tendency of Cd(II) complexes [54].

The identified hydration patterns align with findings in metal, organic frameworks (MOFs), where both intrinsic and additional water molecules play a decisive role in structural stability, porosity, and reactivity [55]. Water molecules may act as structure, directing agents, stabilizers, or catalysts. This effect is particularly relevant in functional applications such as gas adsorption, catalysis, and sensing, where selectivity and functionality are influenced by hydration [56,57].

The varying hydration levels suggest that these complexes can be tailored for specific applications. Complexes with high water content are better suited for water absorption and harvesting. For example, in MOFs like MIL-53, water uptake directly impacts luminescent and sensing properties [58-60]. Conversely, complexes with lower water content may exhibit greater stability in aqueous solutions, making them more reliable for catalytic or electronic applications where structural integrity is crucial [61].

The antibacterial activity of benzophenone oxime (L) and its Metal(II) complexes against *Staphylococcus aureus*, *Salmonella typhi*, and *Escherichia coli* is summarized in Table 7. The results clearly demonstrate that coordination of the ligand with metal ions leads to a general enhancement of antibacterial activity compared with the free ligand. The free ligand exhibited moderate antibacterial effects, producing zones of inhibition in the range of 7-16 mm, whereas the Metal(II) complexes showed significantly improved activity, with inhibition zones reaching up to 23 mm.

Table 7. Antibacterial activity of benzophenone oxime (L) and its Metal(II) complexes.

Isolates	Compounds	Zone of Inhibition (mm)				Standard Ciprofloxacin
		2000µg/ml	1000µg/ml	500µg/ml	250µg/ml	(500µg/ml)
Staphylococcus aureus	Ligand (L)	16 ± 0.4	13 ± 0.6	12 ± 0.4	08 ± 0.5	29 ± 0.6
	$MnL_2(H_2O)_2 \cdot 5H_2O$	18 ± 0.6	14 ± 0.4	12 ± 0.6	10 ± 0.4	29 ± 0.5
	$FeL_2(H_2O)_2 \cdot 5H_2O$	19 ± 0.5	16 ± 0.4	13 ±0.5	10 ± 0.5	29 ± 0.4
	$CoL_2(H_2O)_2 \cdot 6H_2O$	17 ± 0.6	14 ± 0.6	12 ± 0.5	09 ± 0.4	29 ± 0.5
	$CuL_2(H_2O)_2 \cdot 3H_2O$	23 ± 0.7	20 ± 0.6	16 ± 0.4	13 ± 0.5	29 ± 0.6
	$ZnL_2(H_2O)_2 \cdot 5H_2O$	21 ± 0.4	19 ± 0.6	17 ± 0.5	14 ± 0.4	29 ± 0.7
	$CdL_2(H_2O)_2 \cdot 2H_2O$	23 ± 0.6	21 ± 0.4	18 ± 0.6	16 ± 0.6	29 ± 0.7
Salmonella typhi	Ligand (L)	14 ± 0.7	11 ± 0.5	09 ± 0.6	07 ± 0.7	32 ± 0.6
	$MnL_2(H_2O)_2 \cdot 5H_2O$	14 ± 0.7	13 ± 0.4	10 ±0.5	08 ± 0.4	32 ± 0.4
	$FeL_2(H_2O)_2 \cdot 5H_2O$	16 ± 0.6	13 ± 0.5	10 ± 0.7	08 ± 0.4	32 ± 0.6
	$CoL_2(H_2O)_2 \cdot 6H_2O$	22 ± 0.7	21 ± 0.6	16 ± 0.4	08 ± 0.6	32 ± 0.7
	$CuL_2(H_2O)_2 \cdot 3H_2O$	18 ± 0.4	16 ± 0.7	12 ±0.5	10 ± 0.6	32 ± 0.5
	$ZnL_2(H_2O)_2 \cdot 5H_2O$	17 ± 0.4	12 ± 0.4	09 ± 0.5	08 ± 0.7	32 ± 0.7
	$CdL_2(H_2O)_2 \cdot 2H_2O$	20 ± 0.5	17 ± 0.6	14 ± 0.6	12 ± 0.6	32 ± 0.4
Escherichia coli	Ligand (L)	13 ± 0.4	10 ± 0.4	09 ± 0.4	07 ± 0.5	41 ± 0.5
	$MnL_2(H_2O)_2 \cdot 5H_2O$	16 ± 0.6	13 ± 0.5	11 ± 0.5	08 ± 0.4	41 ± 0.7
	$FeL_2(H_2O)_2 \cdot 5H_2O$	14 ± 0.7	12 ± 0.6	10 ± 0.7	09 ± 0.6	41 ± 0.4
	$CoL_2(H_2O)_2 \cdot 6H_2O$	17 ± 0.5	15 ± 0.4	12 ± 0.6	10 ± 0.4	41 ± 0.7
	$CuL_2(H_2O)_2 \cdot 3H_2O$	25 ± 0.7	23 ± 0.5	20 ± 0.4	18 ± 0.7	41 ± 0.4
	$ZnL_2(H_2O)_2 \cdot 5H_2O$	23 ± 0.5	21 ± 0.7	17 ± 0.7	08 ± 0.4	41 ± 0.5
	$CdL_2(H_2O)_2 \cdot 2H_2O$	20 ± 0.7	17 ± 0.5	14 ± 0.4	11 ± 0.7	41 ± 0.4

Note: Values are mean ± SD of three independent experiments (n = 3), L = Ligand ($C_{13}H_{11}NO$).

Among the synthesized complexes, the Cu(II) and Cd(II) complexes displayed the highest antibacterial potency, with maximum inhibition zones of 21 mm and 23 mm, respectively. This enhancement in activity upon metal coordination indicates that the metal center plays a crucial role in modulating the biological performance of the ligand. However, although Cd(II) complexes exhibit notable antibacterial activity, their potential therapeutic application is severely limited due to the well-known toxicity of cadmium. Consequently, the biological results obtained for Cd(II) complexes should be interpreted primarily in terms of structure-activity relationships rather than direct medicinal applicability.

The observed increase in antibacterial activity following complexation is consistent with the chelation theory, which proposes that coordination reduces the polarity of the metal ion through partial sharing of its positive charge with donor atoms of the ligand. This process increases the overall lipophilicity of the complex, thereby enhancing its ability to penetrate bacterial cell membranes. Improved membrane permeability disrupts vital cellular functions such as nutrient transport, respiration, and enzyme regulation, ultimately leading to cell death [62,63].

In addition, the antibacterial behavior of metal complexes is strongly influenced by factors such as coordination geometry, oxidation state, and electronic configuration of the metal center. Cu(II) complexes often adopt square-planar, square-pyramidal, or distorted octahedral geometries, which may facilitate stronger interactions with microbial biomolecules. In contrast, Zn(II) and Cd(II), as d^{10} metal ions, preferentially form tetrahedral geometries due to the absence of ligand field stabilization energy. Such geometrical preferences are well documented for Zn(II) and Cd(II) complexes (e.g., $[ZnCl_4]^{2-}$ and $[Cd(SCN)_4]^{2-}$) and can significantly influence interactions with bacterial enzymes and proteins.

Metal complexes may also exert antibacterial effects through direct interaction with bacterial metalloenzymes, particularly by binding to sulfhydryl (–SH) groups at enzyme active sites. This interaction can inhibit enzymatic activity, leading to loss of essential biological functions and subsequent bacterial growth suppression [64,65]. The combined effects of enhanced lipophilicity, altered coordination geometry, and enzyme inhibition contribute to the superior antibacterial performance observed for the Metal(II) complexes relative to the free ligand.

The results demonstrate that Schiff base Metal(II) complexes exhibit markedly higher antibacterial activity than the uncoordinated ligand. While complexes of biologically relevant metals such as Cu(II) and Zn(II) show promising potential for further medicinal investigation, Cd(II) complexes despite their activity are unsuitable for therapeutic development due to toxicity concerns. Nevertheless, these findings provide valuable insight into structure-activity relationships and highlight the significant influence of metal coordination on the biological behavior of Schiff base ligands.

The antifungal activity of benzophenone oxime (L) and its Metal(II) complexes against Aspergillus flavus and Candida albicans is summarized in Table 8. The results demonstrate that coordination of the Schiff base ligand with transition metal ions significantly enhances antifungal efficacy compared to the free ligand. The uncoordinated ligand exhibited moderate antifungal activity, producing zones of inhibition in the range of 6-15 mm, whereas the Metal(II) complexes showed improved activity, particularly at higher concentrations (2000 µg/mL).

Table 8. Antifungal activity of the ligand and its Metal(II) complexes.

Isolates	Compounds	Zone of Inhibition (mm)				Standard Ketoconazole
		2000µg/ml	1000µg/ml	500µg/ml	250µg/ml	(500µg/ml)
Aspergillus flavus	Ligand (L)	15 ± 0.5	13 ± 0.7	10 ± 0.4	07 ± 0.5	33 ± 0.4
	$MnL_2(H_2O)_2 \cdot 5H_2O$	17 ± 0.4	15 ± 0.7	11 ± 0.5	09 ± 0.7	33 ± 0.5
	$FeL_2(H_2O)_2 \cdot 5H_2O$	16 ± 0.7	14 ± 0.5	13 ± 0.7	10 ± 0.7	33 ± 0.4
	$CoL_2(H_2O)_2 \cdot 6H_2O$	15 ± 0.4	13 ± 0.5	11 ± 0.5	08 ± 0.4	33 ± 0.7
	$CuL_2(H_2O)_2 \cdot 3H_2O$	20 ± 0.5	17 ± 0.4	13 ± 0.7	12 ± 0.4	33 ± 0.5
	$ZnL_2(H_2O)_2 \cdot 5H_2O$	15 ± 0.7	13 ± 0.5	10 ± 0.4	08 ± 0.5	33 ± 0.5
	CdL2(H2O)2·2H2O	18 ± 0.4	16 ± 0.5	14 ± 0.7	11 ± 0.5	33 ± 0.4
Candida albicans	Ligand (L)	12 ± 0.5	10 ± 0.7	08 ± 0.4	06 ± 0.5	27 ± 0.7
	$MnL_2(H_2O)_2 \cdot 5H_2O$	18 ± 0.4	14 ± 0.5	10.7± 0.7	09 ± 0.5	27 ± 0.4
	$FeL_2(H_2O)_2 \cdot 5H_2O$	19 ± 0.7	17 ± 0.7	14 ± 0.7	08.± 0.7	27 ± 0.7
	$CoL_2(H_2O)_2 \cdot 6H_2O$	18 ± 0.4	14 ± 0.4	12 ± 0.5	09 ± 0.5	27 ± 0.5
	$CuL_2(H_2O)_2 \cdot 3H_2O$	16 ± 0.7	14 ± 0.5	12 ± 0.4	08 ± 0.5	27 ± 0.4
	$ZnL_2(H_2O)_2 \cdot 5H_2O$	15 ± 0.4	12 ± 0.7	11 ± 0.4	08 ± 0.4	27 ± 0.5
	CdL2(H2O)2·2H2O	17 ± 0.5	15 ± 0.4	13 ± 0.7	10 ± 0.5	27 ± 0.4

L = Ligand ($C_{13}H_{11}NO$).

Against *Aspergillus flavus*, the Cu(II) complex displayed the highest antifungal activity, with a maximum inhibition zone of 20 mm, followed by the Cd(II), Fe(II), and Mn(II) complexes. Similarly, against *Candida albicans*, the Fe(II) and Mn(II) complexes showed strong antifungal effects, with inhibition zones reaching 19 mm and 18 mm, respectively, while the Cu(II) complex also exhibited notable activity. These results highlight the influence of the metal center on antifungal performance, which depends on both the structural characteristics of the fungal organism and the physicochemical properties of the coordinated metal ion [66,67].

The enhancement of antifungal activity upon metal coordination can be explained by several mechanisms. Chelation reduces the polarity of the metal ion through partial sharing of positive charge with donor atoms, thereby increasing the lipophilicity of the complex. This facilitates penetration through the fungal cell wall and membrane, leading to disruption of cellular structure and function [68,69]. In addition, certain metal complexes particularly those of Cu(II) and Fe(II) can promote the generation of reactive oxygen species (ROS), inducing oxidative stress that damages vital biomolecules such as proteins, lipids, and nucleic acids [70].

Zinc complexes, although less active than Cu(II) and Fe(II) analogues, may exert antifungal effects through nitrosative stress mechanisms, disrupting cellular homeostasis and enzyme function, which explains their moderate antifungal

activity against both fungal strains studied [71]. The observed activity trends are consistent with previous reports demonstrating that Schiff base metal complexes often display superior antifungal properties due to efficient chelation, enhanced membrane permeability, and redox-mediated toxicity [72-75].

Overall, the data indicate that metal coordination significantly improves the antifungal efficacy of benzophenone oxime, with Cu(II), Fe(II), and Mn(II) complexes showing the most pronounced activity. These findings support the continued exploration of Schiff base metal complexes as promising candidates for the development of new antifungal agents, particularly in response to the growing challenge of multidrug-resistant fungal infections [76].

The UV-Vis spectra of the benzophenone oxime ligand (L) and its Metal(II) complexes (Mn, Fe, Co, Cu, Zn, and Cd) are shown in Figure 9. The free ligand exhibits strong absorption bands between 250 and 320 nm, corresponding to π→π transitions of the aromatic benzophenone moiety, and a weaker shoulder around 350-370 nm, assigned to n→π transitions of the oxime group (–C=NOH). Coordination to Metal(II) ions induces notable spectral changes. Mn(II) and Fe(II) complexes display additional bands in the 400-600 nm region, characteristic of d-d transitions, As seen in Figure 9, Co(II) and Cu(II) complexes exhibit broader bands extending to 500-600 nm, reflecting both d-d transitions and possible ligand-to-metal charge transfer (LMCT) [77,78]. In contrast, Zn(II) and Cd(II) complexes show absorption patterns similar to the free ligand, consistent with their d^{10} configuration. Complexation causes slight bathochromic shifts of the π→π* bands for all complexes, indicating increased electron delocalization and stabilization of the ligand's electronic states [79,80]. Further analysis reveals that the intensity and position of these absorption bands are highly sensitive to the coordination environment around the metal ion, providing insights into the geometry and electronic structure of the complexes [78]. Solvent coordination, such as by tetrahydrofuran, can further influence these spectral characteristics, potentially leading to additional bathochromic shifts or altered band intensities [79]. The high extinction coefficients observed for certain intense absorption bands suggest significant contributions from metal-to-ligand charge transfer processes, particularly in cobalt and copper complexes [79,80]. For instance, the electronic absorption spectrum of the Cu complex exhibits bands at 446 and 336 nm, attributed to decreased energy transitions [80]. These spectral changes confirm successful complex formation and imply that metal coordination alters the electronic properties of the ligand, potentially enhancing interactions with microbial biomolecules and antimicrobial activity.

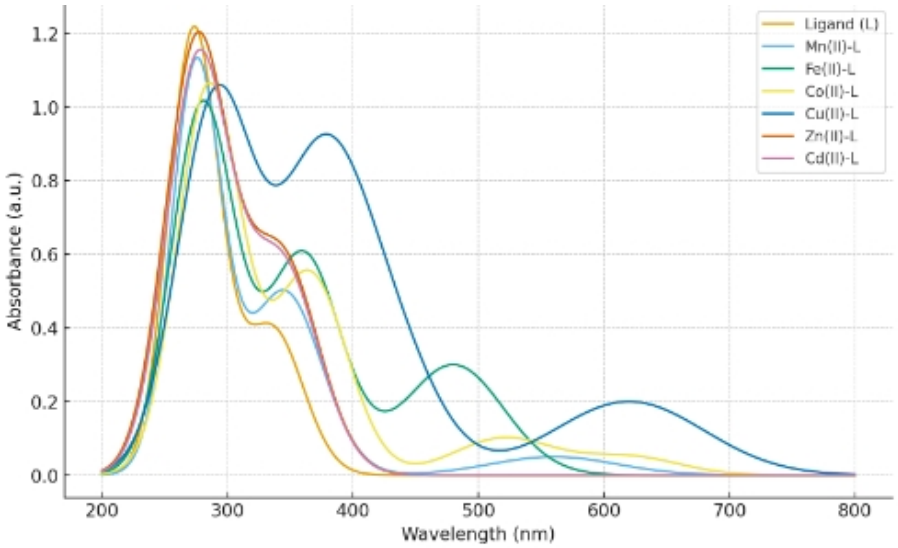

Figure 9. UV-Vis spectra of the benzophenone oxime ligand (L) and its Metal(II) complexes.

Thermogravimetric analysis (TGA) of the benzophenone oxime ligand (L) and its Metal(II) complexes (Mn, Fe, Co, Cu, Zn, Cd) revealed distinct thermal stability patterns across the temperature range of 25-800 °C. The free ligand undergoes a two-step decomposition: an initial mass loss between 200 and 350 °C, likely due to oxime group degradation and partial breakdown of the aromatic framework, followed by gradual decomposition of the residual organic backbone from 350 to 500 °C, leaving approximately 10-25% residual mass at 800 °C. As illustrated in Figure 10, coordination with metal ions significantly increases the initial decomposition temperatures of the complexes compared to the free ligand, indicating enhanced thermal stability.Coordination with metal ions significantly enhances thermal stability, as evidenced by higher initial decomposition temperatures in all complexes. Mn(II) and Fe(II) complexes exhibit broad mass losses between 250 and 400 °C, whereas Co(II) and Cu(II) complexes show sharper degradation around 300-450 °C, suggesting more rigid coordination environments. Zn(II) and Cd(II) complexes demonstrate minimal mass loss below 400 °C, indicative of the stabilizing effect of d^{10} metal centers and strong metal–ligand bonds. Residual masses at 800 °C are higher for all metal complexes, consistent with the formation of thermally stable metal oxides. Further analysis of the TGA curves can provide insights into the activation energies of decomposition for each complex, allowing for quantitative comparison of their thermal stabilities [81,82]. These results indicate that the metal complexes possess thermal robustness suitable for catalytic applications, controlled decomposition in drug delivery, or the synthesis of well-defined metal oxide nanoparticles [83,84].

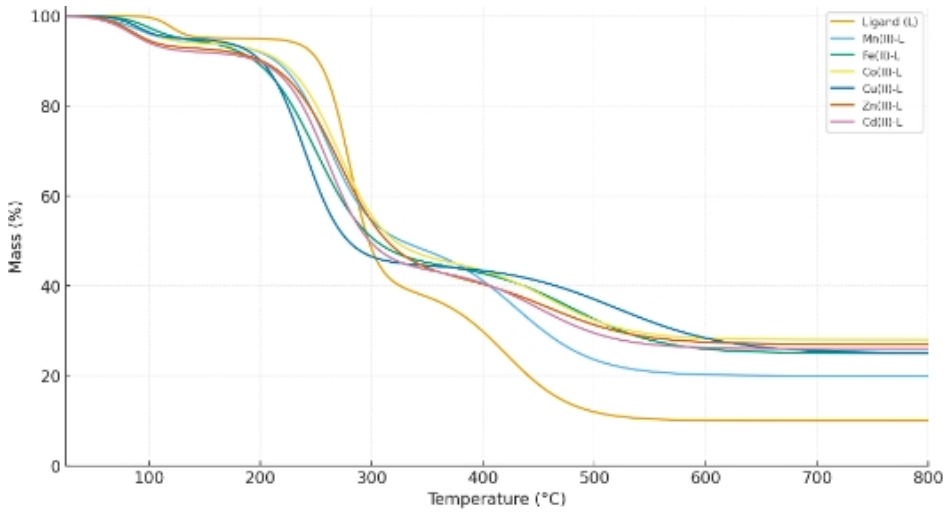

Figure 10. Thermogravimetric analysis (TGA) of the benzophenone oxime ligand (L) and its Metal(II) complexes.

4. Conclusion

A comprehensive study on benzophenone oxime and its Metal(II) complexes with Mn(II), Fe(II), Co(II), Cu(II), Zn(II), and Cd(II) revealed stable coordination with a consistent 1:2 metal, to, ligand stoichiometry. The formation of the complexes was supported by infrared spectroscopy, elemental analysis, and magnetic susceptibility, which indicated coordination through nitrogen and oxygen donor atoms, though definitive structural confirmation would require techniques such as NMR or X, ray crystallography. The complexes displayed enhanced thermal stability (decomposition temperatures 162, 178 °C), preferential solubility in dipolar aprotic solvents, and distinctive electronic and magnetic properties. Antimicrobial screening showed that the metal complexes exhibit superior activity compared to the free ligand against Gram, positive (*S. aureus*), Gram, negative *(E. coli, S. typhi*), and fungal pathogens (*A. flavus, C. albicans)*, likely due to increased lipophilicity and membrane, disruptive properties. These findings position benzophenone oxime Metal(II) complexes as promising candidates for developing new antibacterial and antifungal agents. Future work should include in vivo toxicity assessments, advanced structural elucidation (NMR), and exploration of catalytic or other biomedical applications to fully realize their therapeutic potential.

Conflicts of Interest

The authors declare no conflicts of interest regarding the publication of this article.

Generative AI Statement

The authors declare that no Gen AI was used in the creation of this manuscript.

References

[1] Adaji MU, Iorungwa MS, Salawu OW. Characterization of Schiff base ligand and its metal complexes. Novelties in Schiff Bases, 2024, 7. DOI: 10.5772/intechopen.114182

[2] Hameed A, Al-Rashida M, Uroos M, Abid Ali S, Khan KM. Schiff bases in medicinal chemistry: A patent review (2010-2015). Expert opinion on therapeutic patents, 2017 27(1), 63-79. DOI: 10.1080/13543776.2017.1252752

[3] Wang Y, Wang F, Wang D, Li A, Chen G, Xiong H, et al. Synthesis and structure studies of a new hexavanadate-glycine hybrid with high antitumor activities. Journal of Molecular Structure, 2020, 1201, 127138. DOI: 10.1016/j.molstruc.2019.127138.

[4] Tawfiq KM, Al Naymi HA, Obaid SM, Jarad AJ, Al-Noor TH, Al-Sarray AJ. Synthesis, characterization, molecular docking, cytotoxicity, and antimicrobial activity of Schiff base ligand and its metal complexes. Applied Organometallic Chemistry, 2025, 39(1), e7781. DOI: 10.1002/aoc.7781

[5] Ahmad N, Alam M, Wahab R, Ahmed M, Ahmad A. Synthesis, spectral and thermo-kinetics explorations of Schiff-base derived metal complexes. Open Chemistry, 2020, 18(1), 1304-1315. DOI: 10.1515/chem-2020-0168

[6] Kajal A, Bala S, Kamboj S, Sharma N, Saini V. Schiff bases: A versatile pharmacophore. Journal of Catalysts, 2013, 2013(1), 893512. DOI: 10.1155/2013/893512

[7] Dehnavi MZ, Ostad SN, Abedi A. The influence of the nonleaving group on the anticancer activity of tetrachlorido platinum (IV) complexes with pyridine/bipyridine derivatives. Inorganica Chimica Acta, 2019, 486, 594-601. DOI: 10.1016/j.ica.2018.11.023

[8] Qin W, Long S, Panunzio M, Biondi S. Schiff bases: A short survey on an evergreen chemistry tool. Molecules, 2013, 18(10), 12264-12289. DOI: 10.3390/molecules181012264

[9] Pramodh B, Lokanath NK, Naveen S, Naresh P, Ganguly S, Panda J. Molecular structure, Hirshfeld surface analysis, theoretical investigations and nonlinear optical properties of a novel crystalline chalcone derivative: (E)-1-(5-bromothiophen-2-yl)-3-(p-tolyl)prop-2-en-1-one. Journal of Molecular Structure, 2018, 1161, 9-17. DOI: 10.1016/j.molstruc.2018.01.078

[10] Da Silva CM, da Silva DL, Modolo LV, Alves RB, de Resende MA, Martins CV, et al. Schiff bases: A short review of their antimicrobial activities. Journal of Advanced research, 2011, 2(1), 1-8. DOI: 10.1016/j.jare.2010.05.004
[11] Kouser S, Joythi M, Begum AB, Asha MS, Al-Ostoot FH, Lakshmeesha DP, et al. Molecular docking, synthesis and antimicrobial evaluation of metal complexes with Schiff base. Results in Chemistry, 2023, 5, 100650. DOI: 10.1016/j.rechem.2022.100650
[12] Mills RO, Dadzie I, Le-Viet T, Baker DJ, Addy HP, Akwetey SA, et al. Genomic diversity and antimicrobial resistance in clinical Klebsiella pneumoniae isolates from tertiary hospitals in Southern Ghana. Journal of Antimicrobial Chemotherapy, 2024, 79(7), 1529-1539. DOI: 10.1093/jac/dkae123
[13] Salih KS, Shraim AM, Al, Mhini SR, Al, Soufi RE, Warad I. New tetradentate Schiff base Cu(II) complexes: Synthesis, physicochemical, chromotropism, fluorescence, thermal, and selective catalytic oxidation. Emergent Materials, 2021, 4(2), 423-434. DOI: 10.1007/s42247-021-00183-9
[14] Chakraborty N, Juglan KC, Kumar H. Temperature-dependent thermodynamic and physicochemical studies of glycols in aqueous biotin solutions. Journal of Molecular Liquids, 2021, 337, 116605. DOI: 10.1016/j.molliq.2021.116605
[15] ul Ain Q, Irshad M, Rafique M, Kebaili I, El-Rayyes A. Electrochemical evaluation of Ni-$BaZr_{0.8}Y_{0.1}X_{0.1}O_{3-\delta}$(X=Co, Mn) perovskite anodes synthesized through spinach (green) and oxalic (chemical) assisted auto-combustion routes for IT-SOFCs. RSC advances, 2025, 15(34), 28121-28130. DOI: 10.1039/d5ra03822g
[16] Yamanaka M, Inagaki A, Nakamura E. Theoretical studies on structures and reactivities of Organocuprate(I) and Organocopper(III) species. Journal of Computational Chemistry, 2003, 24(12), 1401-1409. DOI: 10.1002/jcc.10132
[17] Kanahashi K, Urushihara M, Yamaguchi K. Machine learning-based analysis of overall stability constants of metal–ligand complexes. Scientific Reports, 2022, 12(1), 11159. DOI: 10.1038/s41598-022-15300-9
[18] Brandt TG, Tuokkola AR, Yu M, Laine RM. Liquid-feed flame spray pyrolysis enabled synthesis of Co- and Cr-free, high-entropy spinel oxides as Li-ion anodes. Chemical Engineering Journal, 2023, 474, 145495. DOI: 10.1016/j.cej.2023.145495
[19] Sun Y, Dai S. High-entropy materials for catalysis: A new frontier. Science advances, 2021, 7(20), eabg1600. DOI: 10.1126/sciadv.abg1600
[20] Zhao J, Bao J, Yang S, Niu Q, Xie R, Zhang Q, et al. Exsolution-dissolution of supported metals on high-entropy $Co_3MnNiCuZnO_x$: Toward sintering-resistant catalysis. ACS Catalysis, 2021, 11(19), 12247-12257. DOI: 10.1021/acscatal.1c03228
[21] Danilescu O, Bourosh P, Kulikova OV, Chumakov YM, Bulhac I, Croitor L. Dihydrazone Schiff base ligands-appropriate chemosensors for Cd(II) detection. Inorganic Chemistry Communications, 2022, 146, 110199. DOI: 10.1016/j.inoche.2022.110199
[22] Reichardt C, Welton T. Solvents and solvent effects in organic chemistry. John Wiley and Sons, 2011. DOI: 10.1002/9783527632220
[23] Alissa M, Alghamdi A, Alghamdi SA, Alshehri MA, Aloraini GS, Albelasi A, et al. From molecular nanoarchitectonics to device integration: Coordination chemistry in next-generation photonic, electronic, and mechanical technologies. Coordination Chemistry Reviews, 2026, 548, 217187. DOI: 10.1016/j.ccr.2025.217187
[24] Shi W, Guan W, Lei C, Yu G. Sorbents for atmospheric water harvesting: From design principles to applications. Angewandte Chemie, 2022, 134(43), e202211267. DOI: 10.1002/ange.202211267
[25] Guo B, Zhou Z, Sun W, Hu X. High entropy alloys for advanced electrocatalysis with computational insights and multidisciplinary design strategies. iScience, 2025, 28(10), 113577. DOI: 10.1016/j.isci.2025.113577
[26] Ben Youssef M, Poungsripong P, Bidotti H, Abdoul-Yasset H, Gigmes D, Margeat O, et al. Dynamic switching of ferrocene and plasmonic interactions in Au/self-assembled monolayer/single Ag nanocube molecular junctions. The Journal of Physical Chemistry C, 2025, 129(16), 7855-7867. DOI: 10.1021/acs.jpcc.4c07890.
[27] Borase JN, Mahale RG, Rajput SS, Shirsath DS. Design, synthesis and biological evaluation of heterocyclic methyl substituted pyridine Schiff base transition metal complexes. SN Applied Sciences, 2021, 3(2), 197. DOI: 10.1007/s42452-021-04144-z
[28] Nesterova OV, Vassilyeva OY, Skelton BW, Bieńko A, Pombeiro AJ, Nesterov DS. A novel o-vanillin Fe(III) complex catalytically active in C–H oxidation: Exploring the magnetic exchange interactions and spectroscopic properties with different DFT functionals. Dalton Transactions, 2021, 50(41), 14782-14796. DOI: 10.1039/D1DT02366G
[29] Shah SA, Sultan A, Zheng K, Sajjad MT, Baker RT. Evaluation of Cu-and Mn-doped Co_3O_4/NiO composites as cathodes for intermediate temperature solid oxide fuel cells. Journal of Materials Chemistry A, 2025, 13(35), 29486-29503. DOI: 10.1039/d5ta03764f
[30] Gan LL, Tong L, Liu LL, Yue YN, Dong WK. Investigating two structurally different penta-coordinated trigonal bipyramidal Co(II) non-symmetric salamo-type complexes. Journal of Molecular Structure, 2024, 1296(1), 136907. DOI: 10.1016/j.molstruc.2023.136907
[31] Soroceanu A, Bargan A. Advanced and biomedical applications of Schiff-base ligands and their metal complexes: A review. Crystals. 2022, 12(10), 1436. DOI: 10.3390/cryst12101436
[32] Bamigboye M, Wahab O, Deborah S, Ikechukwu E, Mustapha A. Synthesis and characterization of mixed Schiff Base-Salicylic acid metal complexes. EDUCATUM Journal of Science, Mathematics and Technology, 2024, 11(2), 1-7. DOI: 10.37134/ejsmt.vol11.2.1.2024
[33] Balachandran G, Dhamotharan A, Kaliyamoorthy K, Rajammal KS, Kulandaiya R, Raja A. Synthesis, characterization, and catalytic cpplications of Schiff-Base metal complexes. Engineering Proceedings, 2024, 61(1), 26. DOI: 10.3390/engproc2024061026
[34] Wang W, Daran JC, Poli R, Agustin D. OH-substituted tridentate ONO Schiff base ligands and related Molybdenum(VI) complexes for solvent-free (ep) oxidation catalysis with TBHP as oxidant. Journal of Molecular Catalysis A: Chemical, 2016, 416, 117-126. DOI: 10.1016/j.molcata.2016.02.021
[35] Gakiya-Teruya M, Le D, Kumar D, Jen N, Rydberg D, Jo M, et al. Influence of peripheral substituents on Fe(II) spin state in complexes with tridentate Schiff-base ligands. European Journal of Inorganic Chemistry, 2024, 27(31), e202400414. DOI: 10.1002/ejic.202400414
[36] Lavrenova LG, Shakirova OG, Korotaev EV, Trubina SV, Tikhonov AY, Os' kina IA, et al. High-Temperature spin crossover in Iron(II) complexes with 2,6-Bis(1H-imidazol-2-yl) pyridine. Molecules, 2022, 27(16), 5093. DOI: 10.3390/molecules27165093

[37] Ishii T, Ogasawara K, Sakane G. Exploring spin states and ligand field splitting in metal complexes: A theoretical analysis of spin-orbital interactions and magnetic properties. Dalton Transactions, 2024, 53(16), 7175-7189. DOI: 10.1039/D4DT00329B
[38] Dmitriev R, Younas N, Zhang Y, Piryatinski A, Bittner ER. Tensorial spin-phonon relaxation reveals mode-selective relaxation pathways in a single-molecule magnet. arXiv, 2025. DOI: 10.48550/arXiv.2507.17910
[39] Georgiev M, Chamati H. Quantum phase constraints as the origin of zero-field splitting: The case of [Ni (Me_6tren)Cl](ClO_4). Scientific Reports, 2025, 15(1), 11398. DOI: 10.1038/s41598-025-96104-5
[40] Kotaru S, Kahler S, Alessio M, Krylov AI. Magnetic exchange interactions in binuclear and tetranuclear Iron(III) complexes described by spin-flip DFT and Heisenberg effective Hamiltonians. Journal of Computational Chemistry, 2023, 44(3), 367-380. DOI: 10.1002/jcc.26941
[41] Zhang L, Jia J, Yan J. Challenges and strategies for synthesizing high performance micro and nanoscale high entropy oxide materials. Small, 2024, 20(28), 2309586. DOI: 10.1002/smll.202309586
[42] Abubakar S, Shallangwa GA, Ibrahim A. Syntheses and determination of activities of some Metal(II) complexes with derivatives of a novel vanillin-tryptophan Schiff base ligand. Journal of Umm Al-Qura University for Applied Sciences, 2024, 10(4), 613-623. DOI: 10.1007/s43994-024-00129-x
[43] Rashad A, Ibrahim F, Ahmed A, Salman E, Akram E. Synthesis and photophysical study of divalent complexes of chelating Schiff base. Baghdad Journal of Biochemistry and Applied Biological Sciences, 2020, 1(1), 5-17. DOI: 10.47419/bjbabs.v1i01.27
[44] Demehin AI, Oladipo MA, Semire B. Synthesis, spectroscopic, biological activities and DFT calculations of Nickel(II) mixed-ligand complexes of tridentate Schiff bases. Eclética Química, 2020, 45(1), 18-46. DOI: 10.26850/1678-4618eqj.v45.1.2020.p18-43
[45] Ejiah FN, Rofiu MO, Oloba-Whenu OA, Fasina TM. Schiff bases as analytical tools: Synthesis, chemo-sensor, and computational studies of 2-aminophenol Schiff bases. Materials Advances 2023, 4(10), 2308-2321. DOI: 10.1039/D3MA00097D
[46] Hadjiivanov KI, Panayotov DA, Mihaylov MY, Ivanova EZ, Chakarova KK, Andonova SM, et al. Power of infrared and Raman spectroscopies to characterize metal-organic frameworks and investigate their interaction with guest molecules. Chemical Reviews, 2020, 121(3), 1286-1424. DOI: 10.1021/acs.chemrev.0c00487
[47] El Marhraoui K, Laachir A, Guesmi S, Mentre O, Ketatni EM, Bentiss F. New Cadmium(II) coordination complexes based on pentaatomic N-heterocycles and thiocyanate ion as ligands: Synthesis, crystal structure, spectroscopic characterizations, and Hirshfeld surface analysis. Journal of Molecular Structure, 2024, 1316, 138963. DOI: 10.1016/j.molstruc.2024.138963
[48] Morris RH. Reactivity umpolung (reversal) of ligands in transition metal complexes. Chemical Society Reviews, 2024, 53(6), 2808-2827. DOI: 10.1039/D3CS00979C
[49] El-Lateef HM, El-Dabea T, Khalaf MM, Abu-Dief AM. Recent overview of potent antioxidant activity of coordination compounds. Antioxidants, 2023, 12(2), 213. DOI: 10.3390/antiox12020213
[50] Cheng L, Dang Y, Wang Y, Chen KJ. Recent advances in metal-organic frameworks for water absorption and their applications. Materials Chemistry Frontiers, 2024, 8(5), 1171-1194.
[51] Logan MW, Langevin S, Xia Z. Reversible atmospheric water harvesting using metal-organic frameworks. Scientific Reports, 2020, 10(1), 1492. DOI: 10.1038/s41598-020-58405-9
[52] Dinpajooh M, Hightower GL, Overstreet R, Metz L, Henson NJ, Govind N, et al. On the stability constants of metal-nitrate complexes in aqueous solutions. Physical Chemistry Chemical Physics, 2025, 27(18), 9350-9368. DOI: 10.1039/d4cp04295f
[53] Garda Z, Nagy V, Rodríguez-Rodríguez A, Pujales-Paradela R, Patinec V, Angelovski G, et al. Unexpected trends in the stability and dissociation kinetics of Lanthanide(III) complexes with cyclen-based ligands across the lanthanide series. Inorganic Chemistry, 2020, 59(12), 8184-8195. DOI: 10.1021/acs.inorgchem.0c00520
[54] Zahariev F, Ash T, Karunaratne E, Stender E, Gordon MS, Windus TL, et al. Prediction of stability constants of metal–ligand complexes by machine learning for the design of ligands with optimal metal ion selectivity. The Journal of Chemical Physics, 2024, 160(4), 042502. DOI: 10.1063/5.0176000
[55] Sagresti L, Benedetti L, Merz Jr KM, Brancato G. Simulating metal complex formation and dynamics in aqueous solutions: Insights into stability, mechanism, and rates of ligand exchange. arXiv, 2025, 2504.20818. DOI: 10.48550/arXiv.2504.20818
[56] Yu Z, Cao X, Wang S, Cui H, Li C, Zhu G. Research progress on the water stability of a metal-organic framework in advanced oxidation processes. Water, Air, & Soil Pollution, 2021, 232(1), 18. DOI: 10.1007/s11270-020-04953-9
[57] Asghar N, Hussain A, Nguyen DA, Ali S, Hussain I, Junejo A, et al. Advancement in nanomaterials for environmental pollutants remediation: A systematic review on bibliometrics analysis, material types, synthesis pathways, and related mechanisms. Journal of Nanobiotechnology, 2024, 22(1), 26. DOI: 10.1186/s12951-023-02151-3
[58] Chen H, ur Rahman S, Rehman A, Khan AA, Khalid M. Microplastics and antibiotic resistance genes as rising threats: Their interaction represents an urgent environmental concern. Current Research in Microbial Sciences, 2025, 100447. DOI: 10.1016/j.crmicr.2025.100447
[59] Frei A, Verderosa AD, Elliott AG, Zuegg J, Blaskovich MA. Metals to combat antimicrobial resistance. Nature Reviews Chemistry, 2023, 7(3), 202-224. DOI: 10.1038/s41570-023-00463-4
[60] Munteanu AC, Uivarosi V. Ruthenium complexes in the fight against pathogenic microorganisms. An extensive review. Pharmaceutics, 2021, 13(6), 874. DOI: 10.3390/pharmaceutics13060874
[61] Ratia C, Ballén V, Gabasa Y, Soengas RG, Velasco-de Andrés M, Iglesias MJ, et al. Novel Gold(III)-dithiocarbamate complex targeting bacterial thioredoxin reductase: Antimicrobial activity, synergy, toxicity, and mechanistic insights. Frontiers in microbiology, 2023, 14, 1198473. DOI: 10.3389/fmicb.2023.1198473
[62] Sen U, Esteves B, Aguiar T, Pereira H. Removal of antibiotics by biochars: A critical review. Applied Sciences, 2023, 13(21), 11963. DOI: 10.3390/app132111963
[63] Sharma B, Shukla S, Rattan R, Fatima M, Goel M, Bhat M, et al. Antimicrobial agents based on metal complexes: Present situation and future prospects. International Journal of Biomaterials, 2022, 2022(1), 6819080. DOI: 10.1155/2022/6819080
[64] Turner RJ. The good, the bad, and the ugly of metals as antimicrobials. Biometals, 2024, 37(3), 545-559. DOI: 10.1007/s10534-023-00565-y
[65] Vitali V, Zineddu S, Messori L. Metal compounds as antimicrobial agents:‘Smart’ approaches for discovering new effective treatments. RSC advances, 2025, 15(2), 748-753. DOI: 10.1039/D4RA07449A

[66] Wang C, Wei X, Zhong L, Chan CL, Li H, Sun H. Metal-based approaches for the fight against antimicrobial resistance: Mechanisms, opportunities, and challenges. Journal of the American Chemical Society, 2025, 147(15), 12361-12380. DOI: 10.1021/jacs.4c16035
[67] Li J, Pei X. Experimental and theoretical study on the enhanced antifungal activities of tebuconazole after complexation with two zinc salts. Inorganica Chimica Acta, 2025, 574, 122397. DOI: 10.1016/j.ica.2024.122397
[68] Lin Y, Betts H, Keller S, Cariou K, Gasser G. Recent developments of metal-based compounds against fungal pathogens. Chemical Society Reviews, 2021, 50(18), 10346-10402. DOI: 10.1039/D0CS00945H
[69] Lyagin I, Aslanli A, Domnin M, Stepanov N, Senko O, Maslova O, et al. Metal nanomaterials and hydrolytic enzyme-based formulations for improved antifungal activity. International Journal of Molecular Sciences, 2023, 24(14), 11359. DOI: 10.3390/ijms241411359
[70] Mannaa AH, Gomaa EA, Zaky RR, Ghaith EA, Abd El-Hady MN. Bivalent transition metal complexes of triazole pyridine Schiff base with theoretical and biological investigations. Scientific Reports, 2025, 15(1), 31192. DOI: 10.1038/s41598-025-15782-3
[71] Martins N, Rodrigues CF. Biomaterial-related infections. Journal of Clinical Medicine, 2020, 9(3), 722. DOI: 10.3390/jcm9030722
[72] Rubbiani R, Weil T, Tocci N, Mastrobuoni L, Jeger S, Moretto M, et al. In vivo active organometallic-containing antimycotic agents. RSC Chemical Biology, 2021, 2(4), 1263-1273. DOI: 10.1039/D1CB00123J
[73] Contini L, Turner RJ, Grepioni F. Zinc(II), Copper(II) and Silver(I) salicylate-metronidazole complexes as novel antimicrobial agents. Dalton Transactions, 2025, 54(31), 11925-11934. DOI: 10.1039/D5DT01086A
[74] Wahab S, Salman A, Khan Z, Khan S, Krishnaraj C, Yun SI. Metallic nanoparticles: A promising arsenal against antimicrobial resistance–unraveling mechanisms and enhancing medication efficacy. International Journal of Molecular Sciences 2023, 24(19), 14897. DOI: 10.3390/ijms241914897
[75] Kaur R, Kaur K, Alyami MH, Lang DK, Saini B, Bayan MF, et al. Combating microbial infections using metal-based nanoparticles as potential therapeutic alternatives. Antibiotics, 2023, 12(5), 909. DOI: 10.3390/antibiotics12050909
[76] Alselami A, Drummond RA. How metals fuel fungal virulence, yet promote anti-fungal immunity. Disease Models and Mechanisms, 2023, 16(10), dmm050393. DOI: 10.1242/dmm.050393
[77] Gosu NR, Yadav CH, Reddy KR, Losetty V, Kothinti RR, Sampath S. Investigating spectroscopic properties, biological effects, and molecular docking studies of synthesized Schiff base metal complexes. Polyhedron, 2024, 255, 116954. DOI: 10.1016/j.poly.2024.116954
[78] Legendre CM, Lüert D, Herbst-Irmer R, Stalke D. Benchmarking magnetic and spectroscopic properties on highly stable 3d metal complexes with tuneable bis (benzoxazol-2-yl) methanide ligands. Dalton Transactions, 2021, 50(45), 16810-16818. DOI: 10.1039/D1DT03230E
[79] Molla Babaker MM, Khalid M, Al-Mukhtar SE. Synthesis, characterization, and computational study of novel 2-phenoxyethyl xanthate ligand and complexes with some transitions metals. Oriental Journal of Chemistry, 2023, 39(6), 1556. DOI: 10.13005/ojc/390616
[80] Ashraf A, El-Desouky MG, El-Afify MA. Thermal and spectroscopic studies of some prepared metal complexes and investigation of their potential anticancer and antiviral drug activity against SARS-CoV-2 by molecular docking simulation. Biointerface Resarch in Applied Chemistry, 2021, 12(1), 1053-1075. DOI: 10.33263/BRIAC121.10531075
[81] Dhineshkumar E, Rajarajan G, Amala S, Seenivasan M, Rebeiro J. Synthesis and non-isothermal decomposition of Copper(II) complex under dynamic Nitrogen atmosphere. Materials Today: Proceedings, 2021, 42, 700-709. DOI: 10.1016/j.matpr.2020.11.073
[82] Bai X, Yao X, Mohamed HO, Melinte G, Davaasuren B, Hedhili MN, et al. Mitigating coking in Ni-based catalyst for dry reforming through dynamic modulations and high-entropy alloys. SSRN Electronic Journal, 2025. DOI: 10.2139/ssrn.5496061
[83] Prabhakar UP, Periyasami G, Karthikeyan P. Nanostructured metal oxides synthesized via simple thermal decomposition of Co(II), Ni(II), Cu(II), and Zn(II) Schiff base complexes: Characterization and antimicrobial activity. Inorganic Chemistry Communications, 2024, 159, 111796. DOI: 10.1016/j.inoche.2023.111796
[84] Thakur S, Kumar V, Khullar S. Synthesis and characterization of triazole-based coordination polymers using mercapto-succinic acid: Spectroscopic, thermal, and morphological insights. Next Materials, 2025, 8, 100853. DOI: 10.1016/j.nxmate.2025.100853